Naval Research Laboratory

Washington, DC 20375-5000

NRL/MR/4790—92-6983

Simulation of Electron Beam Transport in Ion-Focused Regime Conditioning Cells

R. F. HUBBARD, S. P. SLINKER, R. F. FERNSLER,
G. JOYCE AND M. LAMPE

Beam Physics Branch
Plasma Physics Division

July 21, 1992

REPORT DOCUMENTATION PAGE

Form Approved
OMB No. 0704-0188

1. AGENCY USE ONLY (Leave blank)	2. REPORT DATE	3. REPORT TYPE AND DATES COVERED
	July 21, 1992	

4. TITLE AND SUBTITLE

Simulation of Electron Beam Transport in Ion-Focused Regime Conditioning Cells

5. FUNDING NUMBERS

47-3639-B-2

6. AUTHOR(S)

R. F. Hubbard, S. P. Slinker, R. F. Fernsler, G. Joyce and M. Lampe

7. PERFORMING ORGANIZATION NAME(S) AND ADDRESS(ES)

Naval Research Laboratory
Washington, DC 20375-5000

8. PERFORMING ORGANIZATION REPORT NUMBER

NRL/MR/4790—92-6983

9. SPONSORING/MONITORING AGENCY NAME(S) AND ADDRESS(ES)

NSWC
Silver Spring, MD 20903-5000

DARPA
Arlington, VA 22203

10. SPONSORING/MONITORING AGENCY REPORT NUMBER

11. SUPPLEMENTARY NOTES

12a. DISTRIBUTION/AVAILABILITY STATEMENT

Approved for public release; distribution unlimited.

12b. DISTRIBUTION CODE

13. ABSTRACT *(Maximum 200 words)*

The resistive hose instability can disrupt propagation of self-pinched beams in dense gas. To reduce growth of the instability, beams can be conditioned prior to propagation. The objectives of beam conditioning are to center the beam in order to reduce initial transverse perturbations which seed the hose instability, and to "tailor" the beam emittance in order to detune the head-to-tail coherence of the instability. Emittance tailoring can be performed by transporting the beam through a "passive ion-focused regime (IFR)" cell, which induces a head-to-tail taper of the beam radius; the radius taper is then converted to an emittance taper by passing the beam through a thick exit foil which scatters the beam. Beam centering can be accomplished by transporting the beam through either: (1) a passive IFR cell which is narrow enough to provide wall guiding, or (2) a laser-ionized "active" IFR cell, or (3) a wire cell in which the centering is provided by a current-carrying wire. We report here on axisymmetric particle simulation studies of IFR tailoring cells, alone and in tandem with each of these types of centering cells, and also on the effect of supplementary focusing lenses and conducting foils. We discuss the parameter choices that are conducive to effective beam conditioning. The emphasis is on conditioning configurations and beam parameters that have actually been tested in experiments with the ATA and SuperIBEX accelerators.

14. SUBJECT TERMS

Relativistic electron beam
Emittance tailoring
Ion-focused regime
Resistive hose instability

15. NUMBER OF PAGES

63

16. PRICE CODE

17. SECURITY CLASSIFICATION OF REPORT	18. SECURITY CLASSIFICATION OF THIS PAGE	19. SECURITY CLASSIFICATION OF ABSTRACT	20. LIMITATION OF ABSTRACT
UNCLASSIFIED	UNCLASSIFIED	UNCLASSIFIED	UL

NSN 7540-01-280-5500

Standard Form 298 (Rev 2-89)
Prescribed by ANSI Std Z39-18
298-102

CONTENTS

I. INTRODUCTION 1

II. PASSIVE IFR TAILORING CELLS 6

A. General Description of a Passive IFR Tailoring Cell 6

B. Overview of FRIEZR Simulation Code 9

C. Non-Diverging Beam Injected into a Passive-IFR Cell 12

D. Effects of IFR Entrance Foil and Upstream Focusing Lenses 15

III. MULTI-STAGE CONDITIONING CELLS 18

A. Preionized Channel Centering Cell with Passive IFR Tailoring Cell 19

B. Two-Stage Passive IFR Cells 21

C. IFR and Wire Cell Hybrids 22

IV. MULTI-PULSE IFR CHANNEL PHYSICS 25

V. CONCLUSIONS 28

ACKNOWLEDGMENTS 28

APPENDIX 29

REFERENCES 33

SIMULATION OF ELECTRON BEAM TRANSPORT IN ION-FOCUSED REGIME CONDITIONING CELLS

I. INTRODUCTION

The resistive hose instability[1-18] is the primary factor limiting propagation of high current relativistic electron beams through dense gas in a self-pinched mode. The hose instability is a macroscopic m = 1 kink mode which disrupts the beam by amplifying transverse beam displacements. The quantity $\tau \equiv t - z/c$, which measures the time into the beam pulse at a fixed axial position z, is an approximate constant of the motion for these beams, and thus most theoretical treatments have used z and τ (or, equivalently, $\zeta \equiv c\tau$) as the independent variables instead of z and t. Theory and simulation indicate that the mode is convective in the beam frame, so that at any given time τ into the beam pulse, the transverse displacement $Y(z,\tau)$ grows to a maximum value $Y_{sat}(\tau)$ at some propagation distance $z = z_{sat}(\tau)$, and then decays as the beam propagates to larger z.

The most unstable modes have wavenumber $k \approx 0.7k_\beta \equiv 0.7(2\pi/\lambda_\beta)$, where k_β and λ_β are the betatron wavenumber and wavelength, defined by[1-3]

$$\lambda_\beta \equiv 2\pi/k_\beta \equiv 2\pi a_b(\gamma I_o/I_n)^{1/2}, \qquad (1)$$

where γ is the usual Lorentz factor, a_b is a characteristic beam radius, and I_n is the net current (beam current I_b less plasma return current I_p). The quantity $I_o \equiv mc^3/e$ is 17 kA, independent of beam parameters. (The Alfven limiting current $I_A = \beta\gamma I_o$.) If I_b, I_n, energy $E = \gamma mc^2$, and a_b are all constant in τ, then $k_\beta(\tau)$ is constant throughout the beam, and the instability can grow coherently from the head to the tail of the beam. Theory and simulation then predict many orders of magnitude of hose growth for typical cases of practical interest. In experiments, "raw" beams injected from a beam source into full density air are almost invariably disrupted by hose instability after propagating a few betatron wavelengths.

For many purposes, the evolution of the beam radius $a_b(z,\tau)$ can be adequately described using an envelope model such as the Lee-Cooper equation.[19] This model assumes that the beam expands or contracts self-similarly with the radius a_b given by

Manuscript approved April 29, 1992.

$$\frac{d^2 a_b}{dz^2} = \frac{\epsilon_n^2 - \gamma^2 a_b^2 U}{\gamma^2 a_b^3} , \qquad (2)$$

where ϵ_n is the *normalized* emittance and $U = \langle k_\beta^2 r^2 \rangle = eI_n/\gamma mc^3$ represents the pinching effect of self-magnetic fields. A pinched equilibrium exists when $\epsilon_n^2 = \gamma^2 a_b^2 U$. Equation (2) assumes the beam to be ultrarelativistic ($\gamma >> 1$) and paraxial. The paraxial approximation assumes that the transverse velocity $v_\perp$ of beam particles is much less than the axial velocity $v_z \approx c$. The Lee-Cooper model also formally defines a_b to be the rms radius and $\epsilon_\perp$ to be the associated rms emittance. In addition, if the net current and beam current densities have different radial profiles, I_n should be replaced by the "effective" current I_e,[2,3,19] a radially-weighted measure of the net current within the beam.

If the beam characteristics are such that k_β increases monotonically as a function of τ, the coherence of the hose mode can be destroyed, so that amplification of the mode is substantially reduced.[4-14] It has been recognized for some time that this can be accomplished by tapering the propagating beam from a broad radius at the head to a much narrower radius at the tail.[4-14] It is readily apparent from the pinched equilibrium condition that it is necessary to "tailor" the emittance at injection to insure that $a_b(\tau)$ will be tapered during propagation. Injecting an initially tapered $a_b(\tau)$ into a dense gas, without emittance tailoring, will not lead to a tapered $\lambda_\beta(\tau)$ profile that is maintained during propagation.

Both analytic models[4,8] and simulations[5,7,10-14] clearly demonstrate the effectiveness of emittance tailoring, provided the $a_b(\tau)$ profile is optimized so as to suppress hose throughout the beam, and not just in the head or just in some other part of the beam.

Even with a beam that is properly emittance tailored, several e-folds of hose amplification can be expected in typical cases. Thus, it is also necessary to limit the amplitude of initial transverse perturbations, present in the beam at the point of injection into dense gas, to a small fraction of the beam radius. [Actually, these perturbations can be either displacements $X_o(\tau)$, $Y_o(\tau)$ or transverse velocities (referred to as "drifts") $dX_o(\tau)/dz$, $dY_o(\tau)/dz$.] The frequency content of these perturbations is also important. At any given point in the beam, perturbations with frequency comparable to $\tau_d^{-1}(\tau)$, where

$$\tau_d(\tau) \equiv \pi\sigma_o(\tau)a_b^2(\tau)/2c^2, \qquad (3)$$

is the dipole magnetic decay length, induce strong hose growth.[1] Here $\sigma_o(\tau)$ is the on-axis conductivity, which rises during the early part of the pulse and later saturates due to electron attachment or recombination. High frequency perturbations in the beam head, where τ_d is short, are particularly dangerous. Low frequency displacements do not couple well to hose instability and are relatively benign.

In recent years, conditioning techniques have been developed to tailor the emittance[4-6,11,12,20-27] and center the beam to reduce initial transverse displacements.[26-30] These techniques have been implemented in experiments with the ETA[25,29] and ATA[4,5] accelerators at Lawrence Livermore National Laboratory, SuperIBEX[6,12,22,23,30] and PULSERAD[14] at the Naval Research Laboratory, and IBEX and RADLAC at the Sandia National Laboratories.[26] These experiments offer dramatic evidence of the effectiveness of beam conditioning in stabilizing hose.

The most widely used technique for emittance tailoring involves the use of a "passive ion-focused regime (IFR)" conditioning cell.[20-23] The ion-focused regime refers to propagation of a highly relativistic beam along a plasma channel whose charge density is less than that of the beam.[20-23,31-52] Since $\gamma >> 1$, the repulsive force exerted on the beam by its own radial electrostatic field E_r is essentially canceled by the self-pinch force exerted by the beam's azimuthal magnetic field B_θ. The plasma electrons are ejected radially by E_r, leaving behind a positive ion column which pinches the beam electrostatically. The background gas density must be sufficiently low that the plasma electrons are collisionless and can be easily ejected. If the plasma channel is produced by the beam itself through impact ionization of an initially neutral gas, the process is referred to as passive IFR. If the gas density and beam pulse length are in an appropriate regime,[4,6,11,20-25,31-38] the ion channel density increases significantly during the beam pulse, and therefore the beam radius tapers down throughout the pulse. This radius taper may be converted to an emittance taper by passing the beam through a thick scattering foil on exit from the IFR cell.[4,5,20-23] This process is the primary subject of the present paper; we shall present a variety of axisymmetric simulation studies that demonstrate the dependence of the process on a number of beam and control parameters.

IFR propagation has been studied in other contexts by several investigators, using analytic models,[20,21,35-40,44] axisymmetric simulations,[37-39,45-48] and 3-D simulations[49-52] to study non-axisymmetric effects such as ion hose instability and magnetic erosion.

A variety of techniques have been used to center the beam and thus reduce the perturbations which "seed" the instability. Passive IFR cells exert a centering force due to wall image forces, but the effect is weak if the wall radius is considerably larger than the beam radius, as is necessary if the cell is intended to induce radius tapering. However, it is also possible to propagate a beam in an "active" IFR cell, wherein some external ionization source (e.g., a laser[39-42] or a magnetically-guided low energy electron beam[43]) establishes the plasma channel, and conditions are such that the beam itself does not further ionize the gas significantly. This type of cell exerts a strong centering effect on the beam, and damps transverse perturbations through phase mixing, provided the density profile $n_i(r)$ of the ion channel is not constant within the beam. A third technique is to propagate the beam along either a current-carrying narrow wire[14,26] or an electrostatically-charged resistive wire.[27-29] The highly anharmonic focusing force due to the wire centers the beam and strongly damps transverse perturbations, but can lead to undesirable emittance growth if parameters are not chosen properly. Conditioning cells based on all of these techniques have been employed, in tandem with passive-IFR tailoring cells, in recent experiments. Figures 1 and 2 illustrate the configurations that have been employed. Figure 1a shows a simple passive-IFR tailoring cell, with a thin entrance foil F1 and a thicker exit foil F2 for scattering. Figure 1b shows this cell with an upstream magnetic focusing lens, a configuration that was employed in the ATA experiments to provide additional control over the radius taper $a_b(\tau)$ induced in the cell.[5] Figure 2 shows three configurations for a passive-IFR tailoring cell in tandem with a centering cell: a laser-IFR cell preceding a passive-IFR cell, often used in the ATA experiments (Fig. 2a); a narrow high-density passive-IFR centering cell preceding a broad lower-density passive-IFR cell, used in earlier SuperIBEX experiments[12,23] (Fig. 2b); and a passive-IFR tailoring cell followed by a wire cell, used in more recent SuperIBEX experiments[12,30] (Fig. 2c). We shall present simulation studies of all of these configurations.

It should be noted that if magnetic focusing is used throughout the beamline, as was the case in some ATA experiments, the focusing system can be tuned to minimize the spatial

perturbations $X_o(\tau)$, $Y_o(\tau)$ at the point of injection to the propagation chamber. However, doing so does not effectively suppress hose growth, since the procedure does not minimize the transverse velocities dX_o/dz, dY_o/dz at the same location.

The organization of the paper is as follows. In Sec. II, we present studies of passive-IFR tailoring cells, alone or in combination with focusing lenses or foils. In Sec. III, we present studies of tandem tailoring/centering cells. Section IV discusses the use of passive-IFR tailoring cells in multiple pulse experiments such as the Multi-Pulse Propagation Experiment (MPPE) on ATA.[5] The conclusions are summarized in Sec. V. The Appendix describes modifications to the FRIEZR simulation code[47] that was used for all studies presented here.

II. PASSIVE IFR TAILORING CELLS

A. General Description of a Passive IFR Tailoring Cell

A passive IFR cell[20-23,25,31-38] consists of a chamber filled with low-density gas (typically a few mtorr) in which the beam is propagated for a distance equal to several betatron wavelengths. The channel strength, and therefore the pinch force, increase monotonically with τ, the time into the beam pulse. The very front of the beam head is unpinched, and thus expands at a constant rate characteristic of free expansion, $da_b/dz = \Delta\theta$, where $\Delta\theta$ is the thermal microdivergence in beam electron velocity angles. The weakly pinched beam head expands rapidly, but the beam may need to propagate a long way before the beam head reaches equilibrium at a large radius. In fact, at any given propagation distance z, there will always be a weakly pinched portion of the beam head which is still expanding, and for the typical short lengths of IFR conditioning cells, this expanding region may constitute a substantial fraction of the pulse. The propagation distance required for equilibration decreases as a function of τ. The tail quickly reaches an equilibrium radius that (if entrance conditions are chosen optimally) is comparable to the initial radius. If the cell is long enough, the beam evolves toward an equilibrium in which the radius decreases monotonically as a function of τ. The normalized emittance, $\epsilon_n \equiv \gamma a_b \Delta\theta$, typically will not develop this monotonic taper within the IFR cell; in many cases it is approximately true that $\Delta\theta$ decreases as a_b increases, so that ϵ_n remains roughly constant. However, at the end of the cell the beam is passed through an exit foil which scatters the electrons sufficiently to increase $\Delta\theta$ to a value which is roughly uniform over the duration of the pulse. The radius taper is thus effectively converted to an emittance taper.

A simple, qualitative model of passive IFR conditioning may thus be based on the following assumptions: (1) That ϵ_n is constant within the cell. (2) That ion channel motion may be neglected. (3) That the beam expands self-similarly, and that the beam and channel radial profiles are similar. (4) That $a_b(z, \tau)$ is equal to the smaller of the equilibrium radius $a_{eq}(\tau)$ and the free expansion radius $a_{ex}(z)$. (5) That the beam is neither converging nor diverging at injection, i.e., that $da_b/dz = 0$ at $z = 0$. The resulting analytic model is presented more completely and in a somewhat different form in Ref. 20, and is an extension of a

steady-state model by Briggs.[36] It provides considerable insight and is useful for scaling, although all of these assumptions are of limited validity. In subsequent sections, we shall elaborate on the limitations of these assumptions and use particle simulations to calculate beam evolution more exactly.

With these assumptions, we proceed to calculate the beam radius and emittance, We assume the beam is injected into the IFR cell with radius a_o, thermal microdivergence $\Delta\theta_o$, and normalized emittance $\epsilon_o = \gamma a_o \Delta\theta_o$. The density of ions created by beam-impact ionization is given by[20,36]

$$\partial n_i / \partial \tau = \nu_i n_b, \tag{4}$$

where $n_b(r,\tau,z)$ and $n_i(r,\tau,z)$ are the beam and ion densities, respectively, and ν_i is the gas ionization rate. In air at pressure P, $\nu_i \approx$ P(torr) nsec^{-1}. In the body of the beam, the radius $a_{eq}(\tau)$ is given by the Bennett pinch condition[19,20,26]

$$a_{eq}(\tau) = \epsilon_0 (I_o/\gamma f I_b)^{1/2}, \tag{5}$$

The ratio $f(\tau) \equiv n_i(r = 0,\tau)/n_b(r = 0, \tau)$ is used to characterize the strength of the channel. Equation (5) is the equilibrium solution to the Lee-Cooper envelope equation (2) with I_n replaced by fI_b. The radius $a_{ex}(z) \equiv a_b(\tau = 0, z)$ at the beam head is specified by free expansion,

$$a_{ex} = (a_o^2 + \epsilon_o^2 z^2/\gamma^2 a_o^2)^{1/2} \approx \epsilon_o z/\gamma a_o. \tag{6}$$

The free expansion limit can be obtained from Eq. (2) with U =0, and reduces to the second expression in Eq. (6) when $a_{ex} >> a_o$.[19] If τ_p is defined as some suitable reference point in the body or tail of the beam, the ratio $a_{ex}/a_{eq}(\tau_p)$ may be referred to as the radius tailoring ratio.

In the region of the beam that has reached equilibrium, the microdivergence is given by

$$\Delta\theta_{eq} = (fI_b/\gamma I_o)^{1/2}, \tag{7}$$

and increases monotonically with τ. The beam radius taper is converted to the desired emittance taper by passing the beam through a thick scattering foil located at $z = z_f$. The foil adds a scattering angle $\Delta\theta_{sc}$ to the beam,[19] resulting in a thermal microdivergence given by

$$\Delta\theta^2(z_f) = \Delta\theta_{sc}^2 + \Delta\theta_{eq}^2. \tag{8}$$

The emittance $\epsilon_H(z_f)$ at the beam head after passing through the foil is thus

$$\epsilon_H(z_f) = \frac{\epsilon_o \Delta\theta_{sc} z_f}{a_o}. \tag{9}$$

Similarly, the emittance $\epsilon_T(z_f)$ in the beam tail is

$$\epsilon_T(z_f, \tau) = \epsilon_o \left[\frac{\gamma I_o}{f I_b}\right]^{1/2} \left[\Delta\theta_{sc}^2 + \frac{f I_b}{\gamma I_o}\right]^{1/2}. \tag{10}$$

The ratio $\epsilon_n(z_f, 0)/\epsilon_n(z_f, \tau_p) = \epsilon_H/\epsilon_T$ from (9) and (10) defines an emittance tailoring ratio. To complete the calculation, it is necessary to specify the neutralization fraction $f(\tau)$. For a beam with constant current,[36] $f = \nu_i \tau/2$. For arbitrary $I_b(\tau)$, $\gamma(\tau)$ and $\epsilon_o(\tau)$ profiles at $z = 0$, f can be estimated from[20]

$$f(\tau) = \frac{\nu_i}{2} \frac{\epsilon_o}{\sqrt{\gamma}\, I_b(\tau)} \int_0^\tau d\tau' \frac{\sqrt{\gamma}\, I_b(\tau')}{\epsilon_o}. \tag{11}$$

As an example, consider beam parameters typical of the ATA Multi-Pulse Propagation Experiment[5] (MPPE): $\gamma = 20$, $a_0 = 0.5$ cm, $\epsilon_0 = 0.5$ rad-cm, propagating 60 cm in 10 mtorr of air followed by a scattering foil with $\Delta\theta_{sc} = 0.09$. The ionization rate at this density is $\nu_i = 10^7$ sec^{-1}. From (4) and (9), the radius $a_b(z_f, 0)$ and emittance $\epsilon_n(z_f, 0)$ in the beam head at $z_f = 60$ cm are 3.0 cm and 5.4 rad-cm, respectively. If the beam is 30 nsec long, the tail radius in equilibrium from (8) is 0.49 cm. The final emittance from (9) is $\epsilon_T(z_f) = 1.0$ rad-cm, resulting in a ratio $\epsilon_H/\epsilon_T = 5.4$. This tailoring ratio is in the range considered suitable

for reducing the growth of the resistive hose instability to an acceptable level when the beam is subsequently propagated in dense gas.

B. Overview of FRIEZR Simulation Code

The simple model outlined in the previous section neglects a number of effects which may be treated more precisely using time-dependent envelope codes or full particle simulation codes such as FRIEZR.[47] First, there is a transition region within the beam pulse where the beam is weakly pinched and has not yet reached an equilibrium. In many experimental situations, the tailoring cell is so short that a large fraction of the beam has not yet reached equilibrium at the end of the cell, so the analytical model cannot be relied on for making detailed predictions of emittance tailoring profiles. Full simulation codes such as FRIEZR include a number of physical effects which are usually omitted from simpler models. For example, the FRIEZR code includes beam energy changes arising from the inductive electric field and does not make the ultrarelativistic and paraxial approximations in treating beam dynamics. Particle simulations also allow the beam current density profile to evolve self-consistently and thus do not make the self-similar assumptions used in envelope models. In addition, FRIEZR can treat more complicated beamline configurations and multi-stage conditioning cells. These beamline configurations may include vacuum transport regions with solenoidal fields or discrete focusing lenses as well as centering cells employing preionized plasma channels.

In the remainder of this paper, we concentrate on simulation studies that are chosen to model two recent series of experiments conducted with the ATA accelerator[5] at Lawrence Livermore National Laboratory, and the SuperIBEX beam generator[6,9,12,20,22,30] at the Naval Research Laboratory. In this particular series of ATA experiments, known as the Multi-Pulse Propagation Experiment (MPPE), a train of up to five 10 MeV pulses, separated by several msec,[5] was conditioned and propagated. (Earlier single pulse experiments at ATA used energies in excess of 40 MeV.) SuperIBEX is a single pulse device which produces a 4.5 MeV beam at currents which may exceed 20 kA. Table I lists the beam and conditioning cell parameters used (except as noted specifically in the text) in all of our simulations of these experiments. In all of the simulations, the gas in the IFR tailoring cell was assumed to be air.

(Several other gases as well as air were used in the experiments.) The plasma electrons were assumed in all cases to be ejected instantaneously from the channel.

TABLE I. Beam and IFR cell parameters for analytical and simulation examples.

Parameter	Symbol	Units	ATA	SuperIBEX
Beam energy	γ	-	21	10
Beam current	I_{bo}	kA	6	15
Initial half-current beam radius	a_o, $a_{1/2}(0)$	cm	0.50	0.60
Initial rms beam radius	$a_{rms}(0)$	cm	0.60	0.72
Current rise length	τ_r	nsec	10	10
Pulse length	τ_p	nsec	40	26.7
Initial rms emittance	$\epsilon_o = \epsilon_n(0)$	rad-cm	0.48	1.08
Initial half-current emittance	ϵ_{ho}	rad-cm	0.40	0.90
IFR cell radius	r_w	cm	7.5	2.5 / 5
IFR cell pressure	P	mtorr	2-50	20 / 5-100

The primary quantity of interest from the simulations is the beam radius $a_b(\tau)$ at the IFR cell exit foil. Up to this point, we have been rather cavalier in discussing the "beam radius" a_b. Since pinched beams generally have rounded beam current density profiles $J_b(r)$, there are potentially many ways to define a characteristic beam radius and emittance in particle simulation codes or experimental data. The rms radius a_{rms} is the quantity that appears in the Lee-Cooper definition of emittance.[19] However, the rms radius can be dominated by a small number of beam electrons in a "halo" at large radius. We generally find the half-current radius to be a more useful indication of the beam width. For any specific radial profile, $a_{rms}/a_{1/2}$ has a well-defined value, e.g., ~1.2 for a gaussian. If this ratio becomes large, it is an indication of change in the radial profile, typically with the growth of radial wings.

The beam in FRIEZR is defined by a half-current radius at injection $a_{1/2}(z = 0) = a_o$, nominal beam energy $\gamma_o mc^2$, peak current I_{bo}, current rise time τ_r, pulse length τ_p and initial rms emittance ϵ_o. Beam simulation particles are loaded with a uniform distribution in the the axial variable τ, but the charge on the simulation particles is weighted by $W(\tau) = I_b(\tau)/I_{bo}$. In most cases, the current is assumed to have the form

$$I_b(\tau) = I_o \tanh(\tau/\tau_r), \tag{12}$$

Particles are distributed in the radial direction with an assumed Gaussian current density profile of the form:

$$J_b(r) = \frac{I_b}{\pi a_G^2} \exp(r^2/a_G^2), \tag{13}$$

where a_G and I_b may vary with τ. For a Gaussian, $a_G \approx 1.2a_{1/2}$. [FRIEZR has options for a number of $I_b(\tau)$ and $J_b(r)$ profiles other than those in Eqs. (12) and (13).] The initial normalized transverse velocity $v_\perp/c$ for individual simulation particles is chosen from a Maxwellian distribution with a thermal microdivergence $\Delta\theta_{th}$ which is related to the initial emittance by

$$\Delta\theta_{th} = \epsilon_o/\gamma_o a_{rms}(0). \tag{14}$$

The studies presented here do not include $\gamma(\tau)$ variations which may arise from experimental voltage variations or space charge depression. Space charge depression effects are relatively unimportant for IFR transport in the ATA regime but can be significant for SuperIBEX.[20]

The FRIEZR code uses an unconventional coordinate system which moves at the speed of light with r, t and $\tau = t - z/c$ as the independent variables. (Note that much of the previous literature on FRIEZR and related simulation codes has used $\zeta \equiv c\tau$ rather than τ as the axial coordinate for the distance from the beam head.) The z coordinate does not appear explicitly in the model equations, so z-dependent beamline changes must be transformed to the (r, t, τ) variables using $z = t - c\tau$. Data such as the beam radius or emittance are usually plotted as functions of τ at fixed z-locations in order to facilitate comparisons with time-resolved beam

diagnostics. The implications of this coordinate system and other numerical details are discussed in Ref. 47. The Appendix includes additional discussion of numerics as well as a description of features added specifically to treat conditioning cells. These features include beam impact ionization, channel ion motion, scattering and focusing by thin foils, discrete focusing lenses, and z-dependent wall radius, preionized channel density and/or gas pressure.

FRIEZR has been used to study inductive erosion in preionized channels,[47] wakefield effects in laser propagation through a plasma,[53] beam transport in the ATA[45] and RLA[46] accelerators, beam propagation in passive IFR cells,[37] and both ballistic and pinched propagation in heavy ion fusion target chambers.[54]

C. Non-Diverging Beam Injected into a Passive-IFR Cell

In this section, we consider a simple passive-IFR cell, as shown in Fig. 1a. We continue to assume, for the present, that the beam is neither converging nor diverging at injection, i.e., that $da_b/dz = 0$ at $z = 0$. In so doing, we are neglecting the focusing effect of the entrance foil, and excluding the possibility of a focusing lens upstream. We consider five cases summarized in Table II, each representing a specified variation of the ATA beam of Table I. The beam characteristics at the output end of the tailoring cell ($z = 90$ cm) are summarized in Table II in terms of $a_{1/2}(\tau = 0)$, the half-current radius of the beam head; and $a_{1/2}(\tau = 40\text{nsec})$, $a_{rms}(\tau = 40)$, $\epsilon_n(\tau = 40)$, the half-radius, rms radius, and rms normalized emittance at the beam tail.

In Case 1-A, we specify that the channel ions are stationary, and the initial emittance is roughly matched to the pinch force exerted by the beam-ionized channel. The tail radius thus remains essentially constant, while the rest of the beam expands. Figure 3 shows that the emittance remains reasonably constant throughout the beam. Thus the assumptions of the analytic theory of Sec. II.A are reasonably well satisfied. Indeed, Fig. 4 shows that the output beam radius profile $a_{1/2}(z = 90, \tau)$ agrees well with the analytic theory, particularly in the well-pinched tail.

TABLE II. Summary of FRIEZR simulations of simple passive IFR tailoring cells. Output quantities (last four columns) are at z = 90 cm and $\tau = 0$ (beam head) or $\tau = 40$ nsec (beam tail).

Case	Comment	ϵ_o rad-cm	P mtorr	$a_{1/2}(\tau=0)$ cm	$a_{1/2}(\tau=40)$ cm	$a_{rms}(40)$ cm	$\epsilon_n(40)$ rad-cm
1-A	Fixed ions	0.48	5	2.8	0.48	0.62	0.50
1-B	Low P	0.48	5	2.8	0.38	0.57	0.55
1-C	High P	0.48	20	2.8	0.31	0.55	1.05
1-D	High ϵ_o, P	0.96	20	4.2	0.41	0.61	1.2
1-E	a_o = 1.0 cm	0.96	20	2.0	0.57	0.93	1.95

Case 1-B is similar except that ion dynamics are included (and also in all the remaining cases discussed in this paper). In the beam tail, the ions collapse toward the axis under the influence of the beam's radial electrostatic field.[20,44] For f << 1, the characteristic time scale for ion channel collapse is

$$\tau_c = (\pi a_b/2c)(m_i/m_e)^{1/2}(I_o/I_b)^{1/2}. \qquad (15)$$

The ion collapse increases the strength of the pinch force on the beam, and thus reduces the beam tail radius $a_{1/2}$ at z = 90 cm from 0.48 cm in Case 1-A to 0.38 cm in Case 1-B. This effect is generally desirable, although ion channel motion may also lead to beam degradation through ion hose instability.[20,44,45,51] Figure 5 shows the evolution of $a_{1/2}(\tau)$ as the beam is transported through the IFR cell to z = 30, 90, and 150 cm. In agreement with the analytic model, the head expands freely while the tail rapidly reaches equilibrium. There is a transition region (3 nsec < τ < 17 nsec) where the beam expands at a reduced rate. Figure 6 shows the expansion rate da_{rms}/dz as a function of τ at the same three z-locations. (In this

particular figure, we plot the rms radius rather than the half-current radius.) At $\tau = 0$, the beam continues to expand at a constant rate equal to the free expansion rate. An approximate equilibrium is reached ($da_{rms}/dz \approx 0$) in the tail of the beam, with the equilibrium region moving forward as the beam propagates further in z. Thus the tapered rms radius $a_{rms}(\tau)$ continues to evolve as the beam propagates through a cell of this length. The "equilibrium" radius in the beam tail actually is seen to expand slowly. This occurs for two reasons. First, the strength of the channel ionized by the beam gradually drops as the beam head expands, from its initial value $f \approx \nu_i \tau$ for a pencil beam, toward the Briggs[26] equilibrium value $f \approx \nu_i \tau/2$. Secondly, the collapse of the ion channel causes the beam radial density profile $n_b(r)$ to form a mild halo, which increases the ratio $a_{rms}/a_{1/2}$ from its initial value, and thus increases da_{rms}/dz. It can be seen in Fig. 7 that $a_{rms}/a_{1/2}$ in the tail increases to 1.46, from its initial value of 1.2.

In Case 1-C, the gas density, and therefore the quantity f, which is an index of the pinch strength, are increased by a factor of four. The simple model of Sec. IIA would indicate that $a_{1/2}$ is reduced by a factor of two. However, a more detailed analysis[20] reveals that the beam cannot collapse to an equilibrium radius less than $\sim a_o/\sqrt{2}$; if the initial emittance ϵ_o is too small to balance the pinch force, then the emittance must increase as the beam equilibrates. (The opposite is not true: if ϵ_o is too large to balance the pinch force, the beam can expand with little or no emittance increase.) Indeed, Fig. 8 and Table II show that $a_{1/2}$ collapses to $0.62a_o$, and Fig. 3 clearly shows the emittance increase in the tail that is necessary to prevent further radial collapse. The increase in $a_{rms}/a_{1/2}$ in the tail, from its initial value of 1.2 for a gaussian profile to its final value of 1.8, is an indication of the profile deformation (enhancement of the radial wings) that accompanies the emittance increase. The tailoring induced in this case would not be ideal for typical propagation applications, since the taper is restricted to a small region $\tau \leq 10$ nsec in the head, leaving the remainder of the beam essentially untailored.

In case 1-D, the initial beam parameters are similar to Case 1-C except that the emittance ϵ_o is doubled. As a result, the tail is initially close to equilibrium, and the evolution is similar to Case 1-B but at twice the radius. However, in this case the outer part of the beam head contacts the cell wall at r = 7.5 cm, and is lost. As a result, ϵ_n <u>decreases</u> in

the head, as is seen in Fig. 3. Loss of part of the beam head limits emittance tailoring and is to be avoided in practical implementations.

Case 1-E has the same initial emittance as Case 1-D, but the initial radius a_o is doubled while the initial velocity spread $\Delta\theta$ is halved. As in Case 1-C, the initial emittance is insufficient to support the pinch force in the tail, so that $a_{1/2}$ collapses in the tail to $0.57a_o$, while $a_{rms}/a_{1/2}$ increases to 1.7 (indicative of halo formation), and ϵ_n increases in the tail, as is evident in Fig. 3.

D. Effects of IFR Entrance Foil and Upstream Focusing Lenses

In previous sections, it was assumed that the beam was neither converging nor diverging at entry to the IFR cell, i.e. $da_b/dz = 0$ at $z = 0$ for all beam slices. If a conducting foil is present at entry to the cell, it acts as a focusing lens by shorting out the beam's space charge field.[20,55-58] The focusing angle decreases with γ and is roughly proportional to $I_b(r, \tau)$, the current enclosed within radius r. The focusing strength thus varies with time into the pulse and is nonlinear in r. Foil focusing thus is not easily controlled and tends to be disruptive. However, it is also possible to introduce one or more magnetic lenses in the vacuum transport region ahead of the IFR entrance foil. These lenses can be precisely controlled, and can be used to partially compensate for foil effects or otherwise to fine-tune the radius profile. This method was extensively and successfully employed in the MPPE experiments.[5]

In this section, we present simulations of the conditioning configuration shown in Fig. 1b: a focusing lens L located at z = 6 cm, followed by a vacuum transport region, and then by a passive-IFR tailoring cell with an entry foil F1 at z = 126 cm and a thicker exit foil F2 at z = 176 cm. The beam parameters are representative of the ATA experiments; they are as listed in Table I except that in this section the beam rise time is set to $\tau_r = 20$ nsec, and (in all cases except 2-B) $\epsilon_o = 0.24$ rad-cm. The beam is injected with a relatively large radius a_{inj}. The values of a_{inj} and of the lens focal length f_L are specified in Table III. In all cases except 2-G and 2-J, the entry foil F1 is effectively a 10 mil carbon foil, scattering the beam through an angular spread $\Delta\theta_o = 0.045$ radians.

The results of the simulations are shown in Table III and Figs. 9-13. The effectiveness of the tailoring process may be estimated by comparing the radii $a_{1/2}$ at the end of the IFR cell, given in Table III for τ = 0, 20 and 40 nsec, the head, middle and tail of the beam, respectively.

TABLE III. Summary of FRIEZR simulations using an upstream focusing lens and a 50 cm long passive IFR cell with air at 6 mtorr. All lengths are in cm.

Case	f_L cm	a_{inj} cm	$a_{1/2}(\tau=0)$ cm	$a_{1/2}(20)$ cm	$a_{1/2}(40)$ cm	Comments
2-A	114	1.5	2.25	1.48	1.10	Small a_{inj}; large f_L
2-B	114	1.5	2.6	1.54	1.24	ϵ_o = 0.48 rad-cm
2-C	114	2.0	2.25	1.47	0.84	Small a_{inj}; large f_L
2-D	114	2.5	2.4	1.59	0.92	f_L too large
2-E	114	3.5	2.55	2.05	1.61	Large a_{inj} and f_L
2-F	100	2.5	2.65	1.51	0.64	Near optimum f_L
2-G	90	2.5	2.5	0.99	0.39	$\Delta\theta_{en}$ = 0.031
2-H	90	2.5	2.95	1.44	0.57	Near optimum f_L
2-J	90	2.5	3.4	2.25	1.05	$\Delta\theta_{en}$ = 0.063
2-K	80	2.5	3.2	1.51	0.67	Near optimum f_L
2-L	70	2.5	3.65	1.80	0.92	f_L too short

For these conditions, focal lengths f_L > 100 cm (Cases 2-A through 2-E) lead to poor tailoring. Although the distance between the lens and the entrance foil is 120 cm, Figure 9, which plots $a_{1/2}(z)$ for three beam slices taken from simulation Case 2-D, shows that beam space charge repulsion extends the lens focal length considerably, particularly in the high-current part of the beam (τ = 20 and 40 nsec). Because the entire beam has a large radius and is converging at the IFR entry foil, the beam subsequently overfocuses within the IFR cell

and rebounds, leading to a rather large tail radius (≥0.92 cm) at the exit foil, and insufficient tapering. Note the effect of foil focusing by the IFR entrance foil, which is evident in Fig. 9 as a sudden change in the slope of the $a_{1/2}(z)$ trajectory at z = 126 cm. This foil heats the beam due to both scattering and anharmonic focusing. Beyond this point, the beam is pinched by the ion channel which slows the expansion in the beam body.

Figure 10 plots $a_{1/2}(z)$ for the same three beam slices when the focal length is reduced to 90 cm (Case 2-H). The τ = 4 nsec and 20 nsec beam slices now focus well ahead of the entrance foil while the τ = 40 nsec beam slice focuses just ahead of the foil. This variation in the focal point serves to increase the beam head radius and decrease the minimum radius, thus substantially improving the radius taper after transiting the tailoring cell.

Figure 11 plots $a_{1/2}(\tau)$ just after the final scattering foil for f_L = 70, 90 and 114 cm (Cases 2-L, 2-H and 2-D). The 90 cm focal length produces the smallest beam radius in the body, while the other two cases produce nearly identical results for τ > 23 nsec. The corresponding final emittance profiles are shown in Fig. 12; the f_L = 90 cm case produces an emittance variation of a factor of 3.

The tapered shape of the beam radius $a_{1/2}(\tau)$ is often quite sensitive to the thickness of the IFR entrance foil F1. This effect has been noted in IFR conditioning cell experiments with both MPPE[5] and SuperIBEX.[12,22] Figure 13 plots the final radius $a_{1/2}(\tau)$ for Cases 2-G, 2-H and 2-K, which are similar except for thickness of the IFR cell entrance foil. In these three cases, the entrance foil scattering angle was $\Delta\theta$ = 0.031, 0.045 and 0.063, respectively, corresponding to carbon foil thicknesses of 5, 10 and 20 mils for the 10 MeV MPPE beam. As expected, the thicker foil produces a significantly larger beam radius, but the tailoring is good in all three cases.

III. MULTI-STAGE CONDITIONING CELLS

As we have seen, passive IFR cells can be quite effective in tailoring the beam emittance so as to reduce the growth rate of the hose instability upon subsequent injection into the atmosphere. However, the possibility of instability growth remains, albeit at a lesser rate. Since the beam produced in an accelerator typically has significant transverse fluctuations which can provide the seed for hose growth, it is also necessary to center the beam to damp this type of noise. In order to do this, it is necessary to pass the beam through a centering cell either before or after the IFR tailoring cell. In this section, we shall discuss various options for centering the beam, and the ways in which their compatibility with tailoring cells can be optimized. We shall not study the centering process itself (all of the simulation studies in this paper are axisymmetric), but we shall infer the requirements for and consequences of the centering process. We shall consider three types of centering cells: (A) laser-ionized IFR channels, (B) passive IFR cells with narrow walls, filled with gas at relatively high density, and (C) wire cells.

A. Preionized Channel Centering Cell with Passive IFR Tailoring Cell

In some of the ATA experiments, a KrF laser was used to ionize benzene, in order to create an IFR channel that was used to center a beam.[4,5,39-41,45] In this scheme, the gas density is chosen low enough (< 1 mtorr) so that further ionization of the gas by the electron beam can be neglected. This beam centering technique was at times employed inside the accelerator as well as in a separate centering cell. A passive-IFR tailoring cell, containing gas at higher pressure was located after the centering cell.[4,5] The success of this technique depends on keeping the beam radius narrow at the point of injection to the IFR tailoring cell, and the microdivergence at this point matched to the IFR pinch force.

In Table IV, we summarize the conditions for several FRIEZR simulations that illustrate transport through the complete active IFR/passive IFR conditioning system. In all cases, the laser-IFR cell was 120 cm long, with a pre-ionized channel with radius $a_{ch} = 0.8$ cm. The ion channel density was assumed to have an on-axis density n_{io} and radius $_{ch}$, and the line-integrated channel strength $f_o \equiv N_i/N_b = (\pi n_{io} a_{ch}^2)/(I_{bo}/ec)$. A foil separated

the laser-IFR cell from a passive IFR cell 90 cm in length, filled with air at density 5 mtorr. These conditions were chosen as representative of the MPPE experiment on ATA, and the beam parameters were those chosen in Sec. II.C. to represent the ATA beam, except that $\epsilon_o = 0.36$ rad-cm. (In reality, this configuration was only used on earlier ATA experiments[4] which had beam energies of 40 MeV; an active IFR cell was only used on MPPE in conjunction with a focusing lens and vacuum transport region[5] of the sort described in the previous section.) The results are summarized in Table IV and Figs. 14-16.

TABLE IV. Summary of FRIEZR simulations using a 120 cm long laser-IFR centering cell followed by a 90 cm long passive IFR tailoring cell with air at 5 mtorr. The radius a_{cen} is an average beam radius in the middle of the IFR centering cell (z = 60 cm). The beam head, body and tail radii at the exit of the IFR tailoring cell (z = 210 cm) are denoted by the quantities $a_{1/2}(4)$, $a_{1/2}(20)$ and $a_{1/2}(40)$ which are taken at $\tau = 4$, 20 and 40 nsec, respectively.

Case	f_o	$\Delta\theta_{en}$	a_{cen} cm	$a_{1/2}(4)$ cm	$a_{1/2}(20)$ cm	$a_{1/2}(40)$ cm	Comments
3-A	0.005	0.032	1.20	3.4	1.93	1.48	f_o too small
3-B	0.05	0.032	0.58	3.1	2.2	0.68	Near optimum f_o
3-C	0.15	0.032	0.42	4.0	3.1	1.08	f_o too large
3-D	0.10	0.045	0.39	3.5	2.4	0.67	$\epsilon_o = 0.24$ rad-cm
3-E	0.05	0.045	0.58	3.7	2.8	0.92	Thicker foil
3-F	0.02	0.032	0.54	2.9	2.08	0.68	Near optimum f_o
3-G	Var.	0.032	0.47	2.9	1.85	0.78	$f_o = 0.05$-0.01 ("Laser-timed")

Figures 14 and 15 show $a_{1/2}(\tau)$ at the end of the tailoring cell (z = 210 cm), and the emittance after passing through an exit foil, for three cases. These figures illustrate the effect of varying the ion channel strength f_o in the centering cell. For $f_o = 0.005$ (Case 3-A of Table

IV), the ion channel is so weak that the beam expands to an undesirably large radius $a_{1/2}$ = 1.1 cm in the centering cell. It is underpressured at injection to the tailoring cell. The beam tail expands a bit more in the tailoring cell (due to the focusing effect of the entrance foil); the head, with its low emittance, expands only to $a_{1/2}$ = 3.4 cm by the end of the cell, and the result is a poorly tailored profile with emittance ratio less than 2:1 after passing through the exit foil. In Case 3-B, the laser channel strength f_o = 0.05 is well matched to the subsequent IFR cell. Unlike the previous case, the beam enters the tailoring cell with suitably small radius (~0.6 cm). The tail radius at exit from the tailoring cell is 0.68 cm, close to the injection value, while the head radius increases to 3.1 cm. Figure 15 shows the emittance is well tailored at exit, with a ratio of 3:1 from head to tail. In Case 3-C, the laser channel is so strong, at f_o = 0.15, that the beam emittance increases considerably in the laser-IFR cell. Upon injection to the tailoring cell, the beam is overpressured and expands considerably in the tailoring cell, again leading to poor emittance tailoring.

Figure 16 shows $a_{1/2}(\tau)$ at three different locations, for the successful Case 3-B. At z = 60 cm in the laser-IFR cell, the radius is relatively constant except for an expanded blip at τ = 18 nsec. This perturbation is due to the nearly coherent collapse of the ion channel at this point. This type of ion dynamics must be monitored; it can sometimes (but not in this case) degrade the beam tailoring. At z = 180 cm (60 cm into the tailoring cell), it is evident that the beam head has not had time to expand sufficiently, but by the end of the tailoring cell at z = 210 cm, the tailoring profile is suitable.

There are other parameters available to optimize the matching of the laser-IFR centering cell and the passive IFR tailoring cell. In some experiments at ATA,[4,5] the strength of the laser channel was reduced at the end of the laser-IFR cell, thus causing the beam radius to increase slightly prior to injection into the conditioning cell. (This is done by varying the density of benzene, the laser target gas, as a function of z.) The diverging character of the beam, $da_b/dz > 0$ as the beam strikes the entry foil to the IFR tailoring cell, can be adjusted to improve the tailoring. In the ATA experiments, this technique was used to substantially reduce hose growth when the beam was subsequently propagated in dense gas.[4] In Case 3-G of Table IV, the ion channel strength was ramped down linearly from 0.05 to 0.01 between z = 60 and 120 cm. For these particular parameters, the resulting tailoring profile is found to

be similar to that obtained by having a constant $f_o = 0.02$. At higher tailoring cell pressures, ramping down the channel strength prior to injection into the IFR tailoring cell frequently is found to alter the radius profile substantially.

B. Two-Stage Passive IFR Cells

Fernsler, et al.,[20] have calculated the centering of a beam by a narrow high-density passive IFR cell. A cell of this type has been deployed as the first stage of a two-stage passive IFR cell in experiments with the SuperIBEX beam.[12,23] The configuration is shown schematically in Fig. 2b. In these experiments, the centering cell (first stage) was 80 cm long, with wall radius $a_w = 2.5$ cm, and gas pressure $P_1 = 20$ mtorr. The tailoring cell (second stage) was 40 cm long, with 5 cm wall radius and gas pressure 3-10 mtorr. In some cases, the two sections were separated by a thin foil; in others, an aperture was used in conjunction with differential pumping to maintain the pressure difference between the two stages. We have performed a simulation study of this two-stage conditioning scheme, using these device parameters and SuperIBEX beam parameters as specified in the last column of Table I. We report here on three simulation cases; further details will be reported elsewhere.

In Case 4-A, the pressure in the tailoring cell was $P_2 = 10$ mtorr, and there was no foil (and therefore no scattering or focusing) between the two stages. Case 4-B was similar except that $P_2 = 5$ mtorr. Case 4-C was similar to Case 4-A, except that the two passive-IFR zones were separated by a foil; foil focusing was modeled using the usual thin lens approximation.[57]

Figure 17 shows the beam radius at z = 50 cm (near the middle of the centering cell) and 120 cm (at the exit of the tailoring cell), for the foilless 10 mtorr Case 4-A. There is some tailoring even in the narrow centering cell, and the continued evolution to a tapered profile in the tailoring cell is evident. The final radius taper at z = 120 cm goes from 2.5 cm in the beam head to 0.7 cm at $\tau = 27$ nsec. The flat profile of $a_{1/2}(\tau)$ for $\tau < 6$ ns is indicative of a problem: the head of the beam scrapes the wall of the narrow centering cell, current is lost, and the half-current radius is restricted to $a_{1/2} \approx a_w/\sqrt{2} \approx 1.8$ cm when the beam fills the narrow centering pipe.

Figure 18 compares $a_{1/2}(\tau)$ at the exit of the IFR tailoring cell for the three cases. Case 4-A shows the most satisfactorily tailored profile. In Case 4-B, with tailoring pressure p_2 = 5 mtorr, the beam was mismatched with too large an emittance at injection to the tailoring cell. As a result, the tail expands, and the profile of $a_{1/2}(\tau)$ at exit is rather flat, tapering by only a factor of two from head to tail. The inclusion of foil focusing (Case 4-C) has disastrous consequences. In the low current portion of the beam head (1-3 kA), the effective focal length for the tailoring cell entrance foil is 10 to 30 cm; this limits subsequent beam expansion and is responsible for the large dip in the radius seen at $\tau \approx 8$ nsec. In the high current beam body, the foil focusing effects are much stronger, with the focusing angle $\theta_f \sim 0.2\text{-}0.3$. This part of the beam is overfocused, and expands rapidly after reaching its initial focus, as is evident in Fig. 18 in the region 10 nsec $< \tau <$ 20 nsec. Indeed, the latter half of the beam scrapes the wall of the tailoring cell, resulting in the loss of 3 to 4 kA (in addition to the loss of approximately 2 kA in the centering cell) from the original peak current of 15 kA. This is apparent in the plots of $I_b(\tau)$, at exit from the tailoring cell, shown in Fig. 19 for Cases 4-A and 4-C.

To avoid beam degradation resulting from foil focusing, a "foilless" two-stage IFR cell was designed and installed on SuperIBEX. This configuration used an aperture combined with differential pumping to generate the desired density difference between the two stages. It produced some promising results but often exhibited substantial current loss, and did not usually generate well-tailored pulses. Simulations of this configuration were sensitive to the assumed scale length for the pressure gradient between the two stages; a long gradient scale length often caused substantial current loss near the end of the centering cell in the simulations. The experimental results have been described by Peyser, et al.[23] and Murphy, et al.[30]

C. IFR and Wire Cell Hybrids

In earlier experiments such as those described in Secs. III.A and B, the beam traversed the centering cell first, followed by the IFR tailoring cell, which was terminated with a thick scattering foil to freeze in the emittance tailoring. Since the beam is subject to little or no centering force (particularly in the beam head) in a passive IFR tailoring cell, the beam may

drift off-axis during the tailoring stage, thus amplifying any initial transverse velocity perturbations. These perturbations subsequently couple very effectively to hose instability. Thus, it would be clearly advantageous to center the all of the beam after it has been tailored.

Active wire cells provide an effective means for centering a beam. In such devices, a thin wire carrying a current $I_w \sim (0.1\text{-}0.5)I_b$ provides a strongly anharmonic pinching magnetic field B_w which centers the beam and damps transverse perturbations by phase mixing. The cell may be operated in vacuum or at gas densities as high as 1 atm. In vacuum, the wire produces the same sort of pinch force on an ultrarelativistic beam as a narrow preionized ion channel. (The laser-IFR centering cell on ATA was often referred to as a "wire zone" for this reason.) In practice, it is convenient to operate a wire cell in full density air, but the situation is then complicated by the charge and current distributions induced in the air, and resistive hose instabilities may be excited in the wire cell if the wire current is too low. Wire cells operating in full density air were first developed by Frost[26] and have been deployed on IBEX and RADLAC at Sandia National Laboratories and on SuperIBEX at the Naval Research Laboratory.[12,30] These devices are often referred to as "gas B_θ cells."

In a wire cell, a beam reaches an equilibrium with transverse temperature characterized by a thermal spread $\Delta\theta \approx (2I_w/\gamma I_o)^{1/2}$ where $I_o \equiv 17$ kA. In general, this represents substantial heating of the beam, and is incompatible with the requirement of low beam emittance on entry to a passive IFR tailoring cell unless the wire current is much smaller than the peak beam current. It is not possible for gas B_θ cells to operate in the small I_w regime due to hose instability growth in the wire cell itself. It is possible in principle to operate a vacuum wire cell with very small I_w, but the centering cell length would have to be substantially increased, and the problem of beam drifts in the IFR tailoring cell would persist. Thus, wire cells are generally unsuitable for use prior to an IFR tailoring cell. However, wire cells function very effectively when located after an IFR tailoring cell. In addition to centering the beam, the transverse heating of the beam by the wire converts the radius taper to an emittance taper; it is then not necessary to use a thick scattering foil for this purpose. Simulations of wire cells in both vacuum and gas indicate that the passive-IFR/wire cell configuration is very effective in tailoring, centering, and damping transverse fluctuations on the beam. These results will be discussed in more detail in a future publication. A two-stage

conditioning cell consisting of a passive IFR cell operating at 10 mtorr followed by a gas B_θ-cell with $I_w \approx$ 5-9 kA has recently been installed on SuperIBEX.[12,30] This configuration, which is shown schematically in Fig. 2c, appears to produce well-tailored pulses and shows significant promise in reducing hose instability growth.

IV. MULTI-PULSE IFR CHANNEL PHYSICS

Some potential applications of intense relativistic electron beams require a series or burst of pulses with separation time $\tau_s << 10^{-2}$ sec. These applications include high energy electron beam welding in dense gases[59] and long-range propagation in the atmosphere.[59,60] Questions arise as to possible effects which could make a passive IFR cell unsuitable for multi-pulse applications. For example, does the first pulse leave behind so much plasma that subsequent pulses are adversely affected? Do the early pulses bore a hole in the neutral gas, so that subsequent pulses produce a weaker ion channel? This section discusses the physics of a passive IFR cell in multi-pulse operation and addresses the fundamental question of whether the channel parameters will vary substantially from pulse to pulse.

IFR channel physics for multiple beam pulses can be thought of as proceeding in three stages. The first stage covers the period $\tau < \tau_p$ (typically tens of nsec) during which the electron beam is present. During this stage, the electron beam creates a plasma channel at a rate $\nu_i \approx 10^6$ P where the pressure P is in mtorr.[20,36] Plasma electrons are quickly accelerated to energies of >100 keV by the space charge field of the beam and are radially expelled, leaving behind an ion channel to pinch the beam. This field also causes the ion channel to collapse toward the axis on a time scale τ_c given by Eq. (14). Typically, $\tau_c < \tau_p$, although the collapse time for an individual ion depends on the time history of I_b and a_b after the ion was created. Because of the distribution of ion creation times, ion channel collapse heats the ions to a temperature of the order of the electrostatic potential well. These ions may also produce significant impact ionization.[20] At the end of the first pulse, the typical gas density is several orders of magnitude larger than the beam or ion channel densities, so the plasma is still weakly ionized. At these densities, the plasma electrons have a mean free path of 1-10 m, so they contribute little secondary ionization before they strike the wall.

The second stage occurs after the beam pulse has ended. A hot, positive ion column remains behind. In the absence of collisions and neutralizing electrons, the ion column radius will typically expand to the wall radius within 100 nsec. This effect has been seen in FRIEZR simulations.[46] Charge exchange appears to be the dominant atomic collision process in a multi-pulse IFR cell; in some cases, the mean free path for this process may be

comparable with the beam radius.[61] However, the fast neutrals which it produces tend to be lost to the walls without significantly heating the bulk of the neutral gas. Some plasma electrons may be available to neutralize the expanding ion column, especially if a reservoir of available plasma exists at the IFR cell wall. However, FRIEZR simulations[46] of ion channel motion in the Recirculating Linear Accelerator,[48,62] which has beam and channel densities comparable to those in ATA, indicate that the ion column can be expected to expand to a radius comparable with the tube radius a_w before being neutralized. This occurs because the hot neutralizing electrons which are drawn toward the ion channel have a line density N_e which cannot exceed the ion channel line density N_i and are spread more or less uniformly inside the cell. Thus, their space charge field does not appreciably slow the expansion of the ion column until the ion channel radius is comparable to a_w.

The third stage extends from the time for the ions to expand to the wall (~100 nsec) until the beginning of the next pulse (~1 msec). The above discussion suggests that by the time the next pulse arrives, most of the ions will have either been lost or will be spread throughout the IFR cell. If energy is transferred to neutrals via charge exchange, those particles will presumably be lost to the wall.[61] Very little hole boring will have taken place because all of the relevant mean free paths are much larger than the beam radius. Thus, the next pulse should enter a cell whose neutral density is essentially unchanged from that present during the first pulse.

In summary, if an IFR cell is used to tailor a series of beam pulses separated by ~1 msec, the first pulse will create an IFR plasma column but will not bore a density channel. Substantial plasma may be produced, especially by ejected plasma electrons striking the walls. However, this plasma should not neutralize the ion column until its radius is a substantial fraction of the wall radius. The second pulse may encounter a diffuse plasma, but this should not affect the beam provided the plasma density remains well below that of the channel formed by the second pulse. Thus, we expect subsequent pulses to be tailored in a similar manner to the first pulse.

Beam radius data taken from the Multi-Pulse Propagation Experiment on ATA support this view.[5] A series of five pulses with $\tau_s \approx$ 2-5 msec was injected into a passive IFR cell, and the beam radius profile $a_b(\tau)$ for each pulse was measured after it exited the IFR cell

using light emitted from a quartz foil. The profiles showed little or no variation from pulse to pulse.[5]

V. CONCLUSIONS

Passive IFR cells offer a powerful technique for shaping the radius and emittance profile of an electron beam prior to injection into a dense gas. Even with the simplest configuration, these profiles can be readily adjusted by varying the pressure in the IFR cell, the thicknesses of the IFR entrance and exit foils and the length and radius of the cell. Additional control may be obtained by using a focusing lens ahead of the IFR cell. Passive IFR tailoring cells can also be used in conjunction with other techniques designed to center the beam or damp initial fluctuations. All of these configurations have been simulated with the FRIEZR beam simulation code and have been successfully deployed experimentally.

ACKNOWLEDGMENTS

Many colleagues in the charged particle beam community have contributed to this work. We wish to thank the ATA group at the Lawrence Livermore National Laboratory, including Frank Chambers, William Fawley, Kenneth Struve, Ted Orzechowski, Simon Yu, William Sharp and John Weir, for numerous discussions and for sharing data prior to publication. We also thank the NRL SuperIBEX experimental group, including Robert Meger, John Antoniades, Thomas Peyser, Donald Murphy, Robert Pechacek, Matthew Myers and Jonathan Santos, with whom we have maintained a close collaboration. We also acknowledge numerous conversations with Charles Frost, who pioneered many of the beam conditioning techniques now used on SuperIBEX, and with Dale Welch, Khanh Nguyen, Leon Feinstein, John Wagner, Brendan Godfrey and Steven Swanekamp who have carried out theoretical or simulation studies similar to our own. Finally, we acknowledge the contributions of Jonathan Krall to the FRIEZR simulation code and A. Wahab Ali to our understanding of the atomic physics processes discussed in Section IV.

This work was supported by the Defense Advanced Research Projects Agency, ARPA Order No. 7781, monitored by the Naval Surface Warfare Center and was also supported by the Office of Naval Research.

APPENDIX: FRIEZR SIMULATION CODE

A. General Description

The simulations reported in this paper were performed using the FRIEZR code.[47] FRIEZR is a particle simulation code in which particles are advanced in time t with a fully-relativistic particle pusher. Fields are derived from solutions to the full Maxwell's equations. Ultrarelativistic and paraxial approximations, which are often employed in beam codes, are not used in FRIEZR. However, the axial variable is $\tau \equiv = t - z/c$, rather than z, and the axial grid is divided into slices with uniform width $\Delta\tau$. Relativistic beam particles have nearly constant τ and thus remain within the same beam slice for many time steps. The code is organized so that only particles from one τ-slice are in core at any one time; careful bookkeeping and I/O management are thus required to keep track of particles slipping from one slice to the next. The field equations are solved as functions of r, τ and t, but beam and plasma particles are pushed in Cartesian coordinates. A Courant condition exists which requires the time step Δt and axial grid step $\Delta\tau$ to satisfy $\Delta t \leq \Delta\tau/2$. Typical conditioning cell simulations employ 100-400 beam slices with 500-1000 beam particles per slice. The original code is described in more detail by Krall, et al.[47] This Appendix describes features which have been added specifically to treat IFR conditioning cells. Note that Ref. 47 uses $\zeta = c\tau$ as the axial variable.

The dynamics of plasma electrons and ions occur on very disparate time scales. For high current electron beams, plasma electrons are quickly accelerated radially with velocities which approach c and are thus expelled from the beam on a time scale $\sim a_b/c < 0.1$ nsec. Ions collapse inward on a time scale that is slower by a factor $(m_i/m_e)^{1/2}$. FRIEZR provides for three options for treating plasma particle motion: (1)Use particle simulation to compute electron and ion flow (often very expensive). (2)Freeze the ions and simulate the electron motion (appropriate for short time scales). (3)Assume plasma electrons are instantaneously ejected and use simulation particles to follow the ion motion. The latter approach has been used in the simulations reported in this paper. This assumption makes it much more economical to treat the long beams which are used in present experiments but does not treat inductive erosion.[47]

Creation of plasma by beam impact ionization is an essential feature of passive IFR conditioning cells. In the studies reported here, FRIEZR assumes an ionization cross section $\sigma_i = 10^{-18}$ cm^2 for relativistic electrons impacting neutral gas. A fixed number N_{sp} of simulation plasma electrons and/or ions are created in each axial grid cell at each time step. The plasma particles are created at the instantaneous locations of N_{sp} simulation beam particles which have been selected at random. The charge of the secondary particles is weighted relative to beam particles by

$$W_s = \sigma_i n_g N_{sb} W_{sb} \delta t / c N_{sp}, \qquad \text{(A-1)}$$

where δt is the simulation time step, n_g is the gas density, $W_{sb} = I_b(\tau)/I_{bo}$ is the weight associated with simulation beam particles in a particular τ-slice, and N_{sb} is the number of simulation beam particles in an axial grid cell. Beam-generated ionization causes the plasma density to increase with τ, causing the beam head to be less strongly pinched than the body.

The original FRIEZR code[47] treated propagation in a preionized plasma channel such as that produced by laser ionization of a low density target gas. Such channels were extensively used on ATA.[4,5,39-41,45] FRIEZR generates preionized plasma channels by bringing in new plasma particles into the $\tau = 0$ beam slice at each time step. The laser-produced channel density may also be ramped up experimentally during the electron beam pulse by turning the laser on during the beam pulse. This "laser timing" technique was extensively used on the ATA accelerator to fine-tune the beam pulse.[5,39,45] Since laser timing creates a channel whose density increases during the pulse, the resulting beam radius profile is similar to that produced by beam impact ionization. FRIEZR treats laser timing in the same manner as beam-generated ionization; however, electron-ion pairs are created from a "phantom" set of particle positions chosen to reproduce the radial profile of laser-produced ionization.

Although z is not an independent variable in the FRIEZR code, most time-resolved experimental diagnostics are measured at a fixed z-location. In order to facilitate experimental comparisons, FRIEZR dumps data for each τ-slice at specified "diagnostics stations" at fixed z locations, using the variable change $z = ct - \tau$. The primary quantity of interest in beam conditioning studies is the half-current radius $a_{1/2}(\tau)$, defined as the radius

enclosing 50% of the simulation particles remaining in the system at a given z-location. The rms radius a_{rms} is less useful because it may be strongly influenced by a "halo" of particles at a large radius.[18,45] However, FRIEZR calculates the emittance using the formal definition of Lee and Cooper[19] which is based on the rms radius. The code also calculates a variety of plasma and electromagnetic field quantities.

FRIEZR allows the wall radius, gas density, preionized channel density and axial magnetic field to be varied in a piecewise-linear fashion with z. This capability makes it easy to treat complicated configurations including hybrid conditioning cells such as those described in Section III. In addition, FRIEZR can include discrete beamline elements such as foils and thin magnetic lenses. These may be located at any axial position $z = z_L$. Magnetic lenses are treated by specifying a focal length f_L. As it passes through the lens, each simulation particle is given an impulse $\delta p_x/p_o = -x/f_L$ and $\delta p_y/p_o = -y/f_L$ where x and y are the particle coordinates at $z = z_L$ and $p_o = \gamma_o mc$ is the nominal beam momentum at injection. Magnetic lenses were extensively used to fine-tune the beam taper on ATA.[5]

Foils are widely used to separate different beamline sections. FRIEZR treats scattering by a foil by specifying a characteristic scattering angle $\Delta\theta_{sc}$ based on the foil composition, thickness and nominal beam energy. For example, a titanium foil of thickness T_f (in mils) produces a scattering angle $\Delta\theta_{sc} = T_f^{1/2}/\gamma$. The impulse given individual simulation particles is chosen at random from a gaussian distribution with width $\Delta\theta_{sc}$.

In addition, a conducting foil produces a focusing impulse similar to that produced by a thin lens; this is because the radial electric field E_r produced by the beam is shorted out by the foil. This process has been modeled by Adler,[55] Humphries and Ekdahl[56] and Fernsler, et al.[57] FRIEZR employs a variation of Adler's thin lens approximation to treat foil focusing. The impulse has the form given by[57]

$$\theta_f = -\delta p_r/\gamma mc = F_f(r/a_b)\,(r/a_b)\,I_b/\gamma I_o . \qquad \text{(A-2)}$$

The function $F_f(r)$ is typically 1-3 and varies weakly with r and a_w/a_b and is slightly different for different assumed current density profiles. The effective focal length of this thin "lens" is approximately a_b/θ_f. For high current, moderate energy beams such as those produced by

SuperIBEX, the focusing angle θ_f can be quite steep, and the focal length may be only a few centimeters. This "overfocusing" effect may degrade the beam significantly.[57,58]

A three-dimensional version of FRIEZR, called ELBA,[50,52,63] is capable of treating a variety of effects such as ion hose[43,44,51] and electron hose[52] instabilities which are neglected by FRIEZR. Preliminary results suggest that these effects are not important in passive IFR cells.

REFERENCES

1. E. P. Lee, Phys. Fluids 21, 1327 (1978).

2. M. Lampe, W. Sharp, R. F. Hubbard, E. P. Lee and R. J. Briggs, Phys. Fluids 27, 2921 (1984).

3. W. Sharp, M. Lampe and H. S. Uhm, Phys. Fluids 25, 1456 (1982).

4. W. M. Fawley, Bull. Am. Phys. Soc. 35, 1054 (1990).

5. F. C. Chambers, W. M. Fawley, S. S. Yu and T. E. Orzechowski (private communications).

6. J. Antoniades, M. Myers, D. Murphy, R. Hubbard, T. Peyser, R. Pechacek and R. Meger, "High Current Relativistic Electron Beam Propagation in High Neutral Pressure Environments," in Proceedings of the Eighth IEEE International Pulsed Power Conference, San Diego, 1991 (Institute of Electrical and Electronics Engineers, New York, 1991), p. 585.

7. R. F. Hubbard, S. P. Slinker, R. F. Fernsler, M. Lampe and G. Joyce, Bull. Am. Phys. Soc. 35, 2083 (1990).

8. M. Lampe, R. F. Fernsler, R. F. Hubbard and S. P. Slinker, Bull. Am. Phys. Soc. 35, 2083 (1990).

9. J. A. Antoniades, T. A. Peyser, M. C. Myers, J. Santos and R. A. Meger, Bull. Am. Phys. Soc. 35, 2071 (1990).

10. R. L. Feinstein, D. A. Keeley, E. R. Parkinson and W. W. Rienstra, "Theoretical and Experimental Studies in High Current Beam Physics," Science Applications International Corporation, SAIC-U-74-PA-DOE, 1984.

11. C. Frost and J. Wagner (private communications).

12. R. F. Hubbard, J. A. Antoniades, R. F. Fernsler, M. Lampe, R. A. Meger, D. P. Murphy, M. Myers, R. Pechacek, T. A. Peyser and S. P. Slinker, "Beam Conditioning and Propagation Experiments on SuperIBEX," to appear in Intense Microwaves and Particle Beams III, edited by H. Brandt, SPIE Conference Proceedings No. 1629 (International Society for Optical Engineering, Bellingham, WA, 1992).

13. D. R. Welch, "Particle-in Cell Simulations of the HERMES II Relativistic Electron Beam in Ambient Air," Mission Research Corp.Report MRC/ABQ-N-425 (1989); D. R. Welch, "Analysis of the RADLAC II Lead Pulse Propagation Experiment," Mission Research Corp. Report MRC/ABQ-R-1396 (1991).

14. D. P. Murphy, R. E. Pechacek, D. P. Taggart, R. F. Fernsler, R. F. Hubbard, S. P. Slinker and R. A. Meger, "Electron Beam Tracking in a Preformed Density Channel," submitted to Phys. Fluids B.

15. B. B. Godfrey and D. R. Welch, in Proceedings of the Twelfth Conference on Numerical Simulation of Plasmas, San Francisco (Lawrence Livermore National Laboratory, Livermore CA, 1987), Paper No. CM1.

16. D. R. Welch, F. M. Bieniosek and B. B. Godfrey, Phys. Rev. Lett. 65, 3128 (1990).

17. G. Joyce, R. Hubbard, M. Lampe and S. Slinker, J. Comput. Phys. 81, 193 (1989).

18. R. F. Hubbard, M. Lampe, S. P. Slinker and G. Joyce, Phys. Fluids 31, 2349 (1988).

19. E. P. Lee and R. K. Cooper, Part. Accel. 7, 83 (1976).

20. R. F. Fernsler, R. F. Hubbard and S. P. Slinker, "Conditioning Electron Beams in the Ion-Focused Regime," submitted to Phys. Fluids B.

21. R. F. Fernsler, R. F. Hubbard, S. P. Slinker, M. Lampe and G. Joyce, Bull. Am. Phys. Soc. 35, 2083 (1990).

22. J. Antoniades, M. Myers, D. Murphy, T. Peyser, R. Hubbard, R. Fernsler, R. Pechacek and R. Meger," IFR Cell Radius Tailoring on SUPERIBEX," in Proceedings of the Eighth IEEE International Pulsed Power Conference, San Diego, 1991 (Institute of Electrical and Electronics Engineers, New York, 1991), p. 582.

23. T. A. Peyser, J. A. Antoniades, M. C. Myers, D. P. Murphy, R. E. Pechacek and R. A. Meger, Bull. Am. Phys. Soc. 35, 2071 (1990).

24. D. J. Weidman, M. J. Rhee, H. S. Uhm and K. T. Nguyen, "Intense Electron Beam Radius-Tailoring Experiment," to appear in Intense Microwaves and Particle Beams III, edited by H. Brandt, SPIE Conference Proceedings No. 1629 (International Society for Optical Engineering, Bellingham, WA, 1992).

25. K. W. Struve, E. J. Lauer and F. W. Chambers, in Proceedings of the Fifth International Topical Conference on High Power Particle Beams, San Francisco, 1983 (Lawrence Livermore National Laboratory, Livermore, CA, 1983), p. 408.

26. C. A. Frost, S. L. Shope, G. T. Leifeste, and D. Welch, Bull. Am. Phys. Soc. 35, 933 (1990); C. Frost and D. Welch (private communications).

27. R. F. Fernsler and P. Boris, in Beams 88: Proceedings of the Seventh International Conference on High Power Particle Beams, Karlsruhe, Germany (Kernforschungszentrum Karlsruhe GmbH, Karlsruhe, Germany, 1988), p. 900.

28. W. A. Barletta and R. J. Briggs, in Proceedings of the Fifth International Topical Conference on High Power Particle Beams, San Francisco, 1983 (Lawrence Livermore National Laboratory, Livermore, CA, 1983), p. 350.

29. D. S. Prono, G. J. Caporaso, A. G. Cole, R. J. Briggs, Y. P. Chong, J. C. Clark, R. E. Hester, E. J. Lauer, R. L. Spoerlein and K. W. Struve, Phys. Rev. Lett. 51, 723 (1983).

30. D. P. Murphy, R. E. Pechacek, T. A. Peyser, J. A. Antoniades, M. D. Myers, R. F. Fernsler, R. F. Hubbard and R. A. Meger, "Relativistic Electron Beam Tracking of Reduced Density Channels in Normal Density Air," in Proceedings of the Eighth IEEE International Pulsed Power Conference, San Diego, 1991 (Institute of Electrical and Electronics Engineers, New York, 1991), p. 589.

31. S. E. Graybill and S. V. Nablo, Appl. Phys. Lett. 8, 18 (1966).

32. R. J. Briggs, R. E. Hester, E. J. Lauer, E. P. Lee and R. L. Spoerlein, in Proceedings of the Second International Conference on Higher Power Electron and Ion Beam Research and Technology, Ithaca, NY, (Cornell University Press, Ithaca, NY, 1977), p.319.

33. M. A. Wilson, IEEE Trans. Plas. Nuc. Sci. NS-28, 3375 (1981).

34. K. T. Nguyen, R. F. Schneider, J. R. Smith and H. S. Uhm, Appl. Phys. Lett. 50, 239 (1987).

35. See NTIS Document No. DE82000242/LL "Modeling Beam Front Dynamics at Low Gas Pressures", by R. J. Briggs and S. S. Yu, Lawrence Livermore National Laboratory, UCID-19399 (1982). Copies may be ordered from the National Technical Information Service, Springfield, VA 22161. The price is $12.50 plus $3.00 handling fee. All orders must be prepaid.

36. See NTIS Document No. DE82016636/LL, "A Simple Model of Beam Transport in Low Pressure Ion-Focused Regimes," by R. J. Briggs, Lawrence Livermore National Laboratory, UCID-19187 (1981). Copies may be ordered from the National Technical Information Service, Springfield, VA 22161. The price is $17.00 plus $3.00 handling fee. All orders must be prepaid.

37. R. F. Hubbard, G. Joyce, J. Krall, S. P. Slinker and M. Lampe, Bull. Am. Phys. Soc. 32, 1718 (1987).

38. S. B. Swanekamp, Ph.D. Dissertation, Univ. of Michigan, Ann Arbor, MI (1990).

39. W. M. Fawley, J. K. Boyd, G. J. Caporaso, F. W. Chambers, Y. P. Chong, P. Lee, T. J. Orzechowski, D. R. Rogers, K. W. Struve, J. T. Weir and J.S. Hildum, in Proceedings of the 1989 IEEE Particle Accelerator Conference, Chicago, 1989 (Institute of Electrical and Electronics Engineers, Piscataway, NJ, 1989), p. 1489.

40. G. J. Caporaso, in Proceedings of the 1987 IEEE Particle Accelerator Conference, Washington, 1987 (Institute of Electrical and Electronics Engineers, Piscataway, NJ, 1987), p. 1001.

41. W. E. Martin, G. J. Caporaso, W. M. Fawley. D. Proznitz and A. G. Cole, Phys. Rev Lett. 54, 685 (1985).

42. R. F. Lucey, R. M. Gilgenbach, J. E. Tucker and C. L. Enloe, Laser and Part. Beams 6, 687 (1988).

43. K. J. O'Brien, G. W. Kamin, T. R. Lockner, J. S. Wagner, I. R. Shokair, P. D. Kiekel, I. Molina, D. J. Armstead, S. Hogeland, E.T. Powell, and R. J. Lipinski, Phys. Rev. Lett. 60, 1278 (1988).

44. H. L. Buchanan, Phys. Fluids 30, 221 (1987).

45. R. F. Hubbard, G. Joyce, S. P. Slinker, J. Krall and M. Lampe, in Beams 88: Proceedings of the Seventh International Conference on High Power Particle Beams, Karlsruhe, Germany (Kernforschungszentrum Karlsruhe GmbH, Karlsruhe, Germany, 1988), p. 906.

46. R. F. Hubbard, G. Joyce and S. P. Slinker, Bull. Am. Phys. Soc. 34, 1997 (1989).

47. J. Krall, K. Nguyen and G. Joyce, Phys. Fluids B 1, 2099 (1989).

48. M. A. Mostrum and D. Mitrovich, "ARCTIC - A Frozen Field Code for Investigating Ion-Focused Beam Transport," Mission Research Corporation, AMRC-R-1001 (1987).

49. T. P. Hughes, in Proceedings of the 1987 IEEE Particle Accelerator Conference, Washington, DC (Institute of Electrical and Electronics Engineers, Piscataway, NJ, 1987), p. 945.

50. R. F. Hubbard, G. Joyce and S. P. Slinker, in Proceedings of the Conference on Computer Codes and the Linear Accelerator Community, Los Alamos, NM (Los Alamos National Laboratory, Los Alamos, NM, 1990), p. 317.

51. See NTIS Document No. DE89002997/LL, "Analysis and Benchmarking Calculations for the BUCKSHOT Code," by I. R. Shokair and J.S. Wagner, Sandia National Laboratories, SAND87-2015 (1988). Copies may be ordered from the National

Technical Information Service, Springfield, VA 22161. The price is $17.00 plus $3.00 handling fee. All orders must be prepaid.

52. D. H. Whittum, W. M. Sharp, S. S. Yu, M. Lampe and G, Joyce, Phys. Rev. Lett. 67, 991 (1991).

53. P. Sprangle, E. Esarey, A. Ting and G. Joyce, Appl. Phys. Lett. 53, 2146 (1988).

54. R. F. Hubbard, M. Lampe, G. Joyce, S. P. Slinker, I. Haber and R. F. Fernsler, Part. Accel. 37-38, 161 (1992).

55. R. J. Adler, Part. Accel 12, 39 (1982).

56. S. Humphries, Jr., and C. Ekdahl, J. Appl. Phys. 3, 583 (1988).

57. R. F. Fernsler, R. F. Hubbard and S. P. Slinker, J. Appl. Phys. 68, 5985 (1990).

58. J. A. Antoniades, R. A. Meger, T. A. Peyser, M. C. Myers, S. Humphries, Jr., and C. Ekdahl, "High-Current Beam Transport Experiments Using Foil Focusing," in Proceedings of the Seventh IEEE International Pulsed Pcwer Conference, Monterey, CA, 1989 (Institute of Electrical and Electronics Engineers, New York, 1989), p. 931.

59. E. Nolting and A. C. Smith (private communications).

60. See, for example, G. Bekefi, B. T. Feld, J. Parmentola and K. Tsipis, Nature 284, 219 (1980).

61. A. W. Ali (private communication).

62. S. L. Shope, W. K. Tucker, D. E. Hasti, J. W. Poukey, G. W. Kamin and W. W. Rienstra, in Proceedings of the 1987 IEEE Particle Accelerator Conference, Washington, DC, 1987, (Institute of Electrical and Electronics Engineers, New York, 1987), p. 917.

63. G. Joyce, J. Krall and S. P. Slinker, in Proceedings of the Conference on Computer Codes and the Linear Accelerator Community, Los Alamos, NM (Los Alamos National Laboratory, Los Alamos, NM, 1990), p. 99.

FIGURE CAPTIONS

FIG. 1. Schematic diagrams of IFR tailoring cell configurations. Simple passive IFR cell (a) uses a thin entrance foil (F1) and a thicker exit foil (F2). the region between the two foils contains a low density gas. In configuration (b), the IFR cell is preceded by a vacuum transport region with a focusing lens to control the rate of beam expansion at the entrance foil (F1).

FIG. 2. Schematic diagrams of IFR tailoring cells combined with various centering cells. The active IFR / passive IFR configuration (a) employs a centering cell with a plasma channel (CH) created by a laser or low energy electron beam. The two-stage passive IFR cell (b) uses a passive IFR cell with a higher gas density and smaller wall radius to center the beam prior to injection into the tailoring cell. The IFR / wire cell hybrid configuration (c) uses a current-carrying wire (W) to center the beam after it has been tailored. The foils (F1-F3) may be relatively thin. The wire cell may be operated in vacuum or in full density air.

FIG. 3. Normalized emittance $\epsilon_n(\tau)$ at z = 90 cm for Cases 1-A, 1-B, 1-C, 1-D and 1-E. Emittance for Cases 1-A, 1-B and 1-D remain near their injected values except for cooling due to particle loss in the beam head seen in Case 1-D. Cases 1-C and 1-E both show emittance growth in beam body due to overpinching by the strong ion channel.

FIG. 4. Comparison of beam radius from fixed ion FRIEZR simulation Case 1-A with the corresponding analytical solution from Eqs. (5) and (6).

FIG. 5. Beam half-current radius $a_{1/2}(\tau)$ at z = 30, 90 and 150 cm for Case 1-B. The beam head expands freely while the body is nearly in equilibrium.

FIG. 6. Beam expansion rate da/dz versus τ at z = 30, 90 and 150 cm for the case shown in Fig. 5.

FIG. 7. Plot of beam half-current and rms radii $a_{1/2}$ and a_{rms} versus τ at z = 90 cm from FRIEZR simulation Case 1-B. IFR cell pressure is 5 mtorr.

FIG. 8. Plot of $a_{1/2}(\tau)$ and $a_{rms}(\tau)$ at z = 90 cm for the 20 mtorr IFR cell Case 1-C. Beam radius contracts more quickly in the beam head and is essentially constant for $\tau > 20$ nsec.

FIG. 9. Evolution of beam radius $a_{1/2}(z)$ at τ = 4, 20 and 40 nsec from simulation Case 2-D. Nominal focal length for the upstream lens is 114 cm. The slice in the beam head (τ = 4 nsec) reaches its minimum radius near the geometric focal point, while later slices focus further downstream due to space charge effects. This results in a relatively large minimum beam radius at the IFR exit foil. Note that this figure was reconstructed from $a_{1/2}(\tau)$ data dumped at a small number of z-locations, so the gridding in the code ($c\Delta t$ = 1.5 cm) is much smaller than that indicated in the figure.

FIG. 10. Beam radius $a_{1/2}(z)$ for the same three slices for a simulation with f_L reduced to 90 cm (Case 2-H). This causes the beam body to focus near the IFR entrance foil, resulting in a smaller minimum radius at the IFR exit foil.

FIG. 11. Beam radius profile $a_{1/2}(\tau)$ at the IFR exit foil for upstream focal length f_L = 70, 90 and 114 cm (Cases 2-L, 2-H and 2-D). Optimal tailoring is exhibited by the f_L = 90 cm case.

FIG. 12. Emittance profile $\epsilon_n(\tau)$ at the IFR exit foil for the three cases shown in Fig. 11.

FIG. 13. Effect of the IFR entrance foil scattering angle on the beam radius profile $a_{1/2}(\tau)$ at the IFR exit foil. Scattering angle $\Delta\theta_{en}$ = 0.031, 0.045 and 0.063 for the three simulations (Cases 2-G, 2-H and 2-J).

FIG. 14. Beam radius $a_{1/2}(\tau)$ at the end of the tailoring cell for three different values of the laser-IFR cell channel strength f_o. Simulation cases are 3-A, 3-B and 3-C. Best results are

obtained with the intermediate value $f_o = 0.05$ (Case 3-B). Both strong and weak channel cases result in a larger final radius and a less desirable tailoring profile.

FIG. 15. Emittance profile $\epsilon_n(\tau)$ at the end of the tailoring cell for the three simulations shown in Fig. 14.

FIG. 16. Plot of beam radius $a_{1/2}(\tau)$ at three different locations from a simulation of a laser-IFR centering cell followed by a passive IFR tailoring cell (Case 3-B). The z = 60 cm curve is in the middle of the centering cell, while the other two locations are at possible locations for the IFR exit foil.

FIG. 17. Simulation of a SuperIBEX "foilless" two-stage IFR cell with $P_1 = 20$ mtorr and $P_2 = 10$ mtorr (Case 4-A). The z = 50 cm location is near the middle of the centering cell, while z = 120 cm is at the end of the tailoring cell. The final radius profile $a_{1/2}(\tau)$ exhibits fairly good tailoring, but has a substantial region in the beam head where it is relatively flat.

FIG. 18. Comparison of the beam radius profile at the tailoring cell exit for two-stage IFR simulations 4-A, 4-B and 4-C. Case 4-B has P_2 reduced to 5 mtorr, resulting in a relatively flat tailoring profile and a larger minimum radius. Case 4-C is a repeat of the $P_2 = 10$ mtorr Case (4-A) but includes the effects of foil focusing. The inclusion of foil focusing degrades the beam radius profile significantly.

FIG. 19. Comparison of the transported current $I_b(\tau)$ at the tailoring cell exit for simulations with and without foil focusing (Cases 4-C and 4-A). The current loss seen in presence of the foil is due to an overfocusing effect which causes the beam to expand rapidly in the tailoring cell following its initial collapse after passing through the foil.

(a) Simple Passive IFR Cell

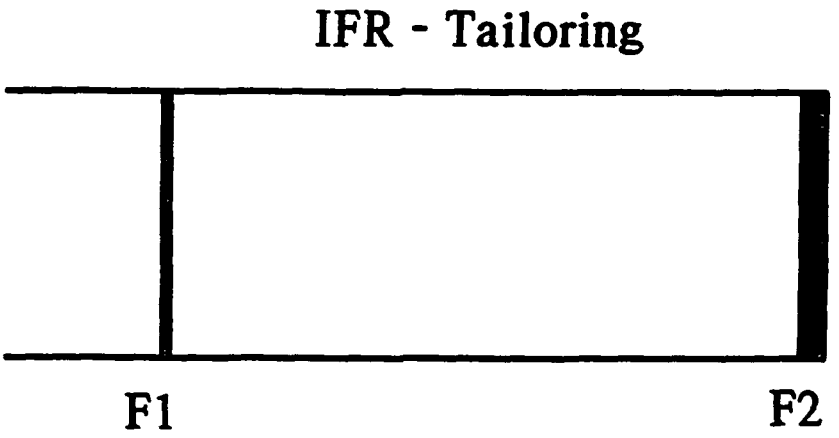

(b) Passive IFR Cell with Upstream Lens

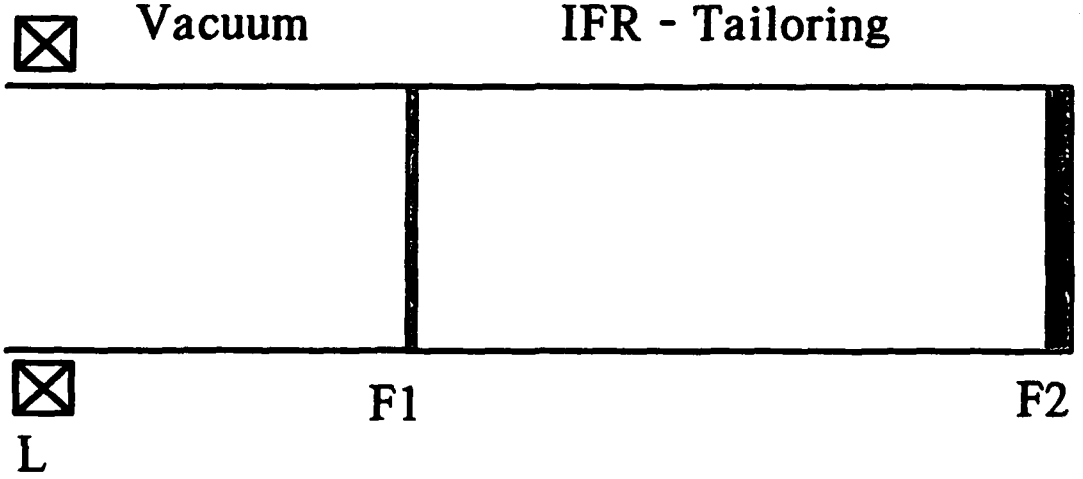

Figure 1

(a) Active IFR/Passive IFR Cell

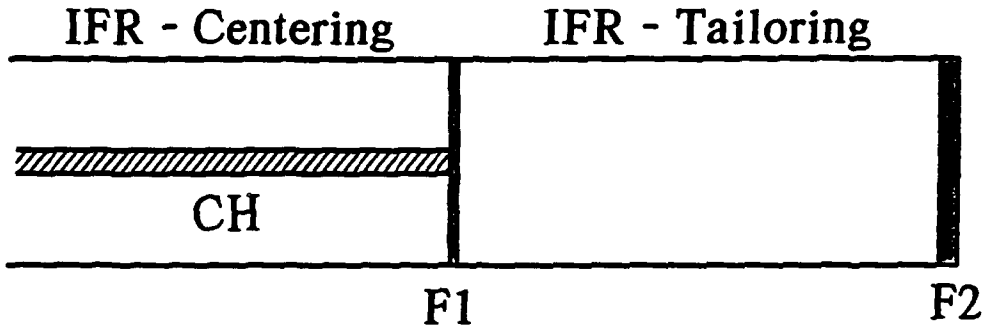

(b) Two-Stage Passive IFR Cell

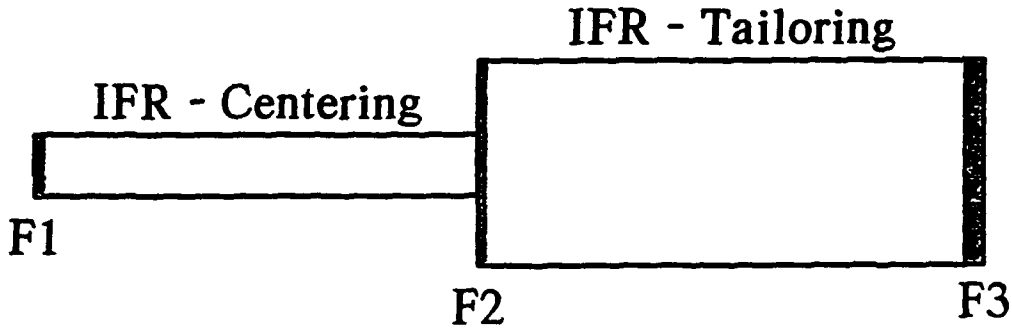

(c) IFR/Wire Cell Hybrid

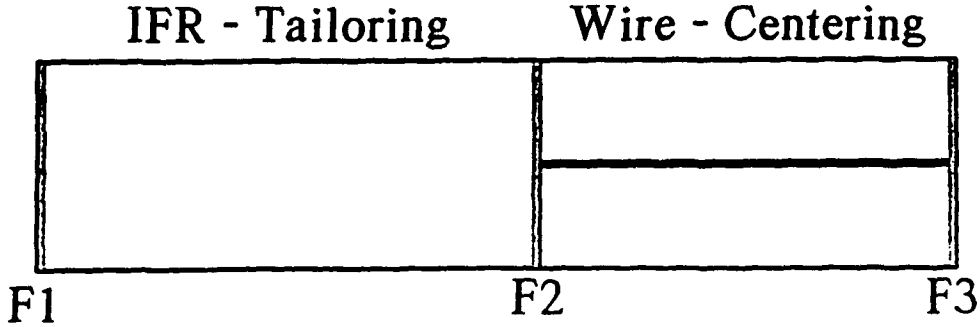

Figure 2

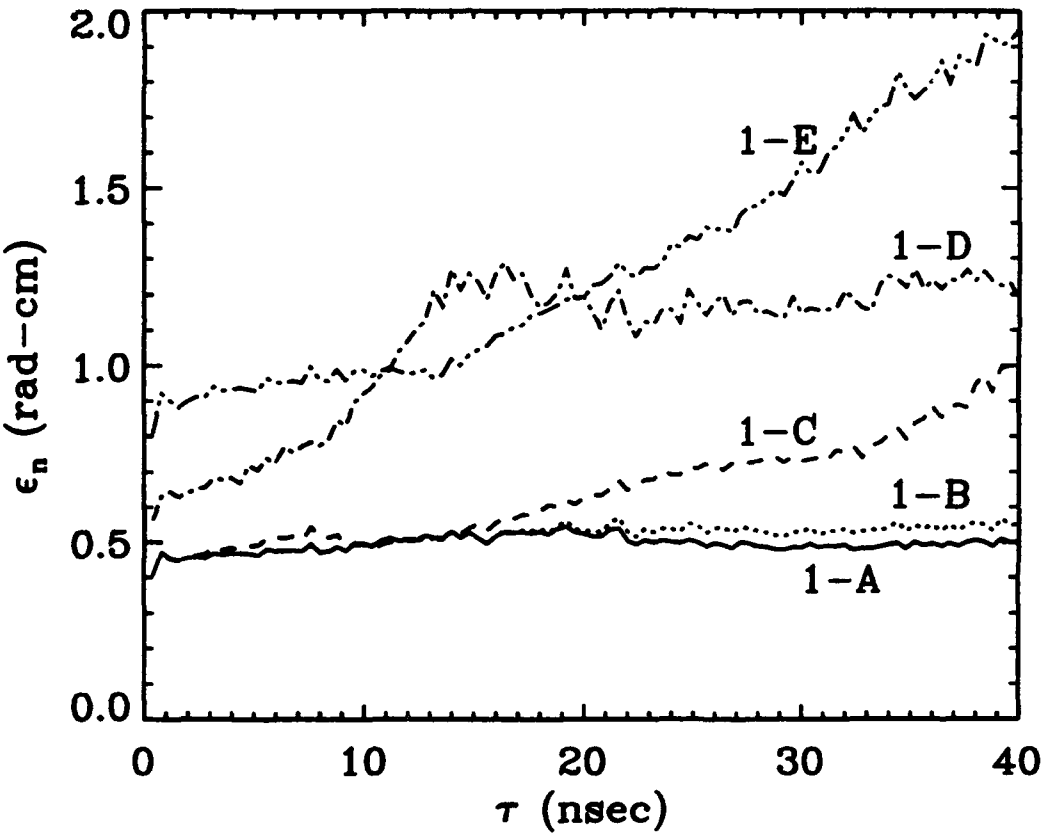

Figure 3

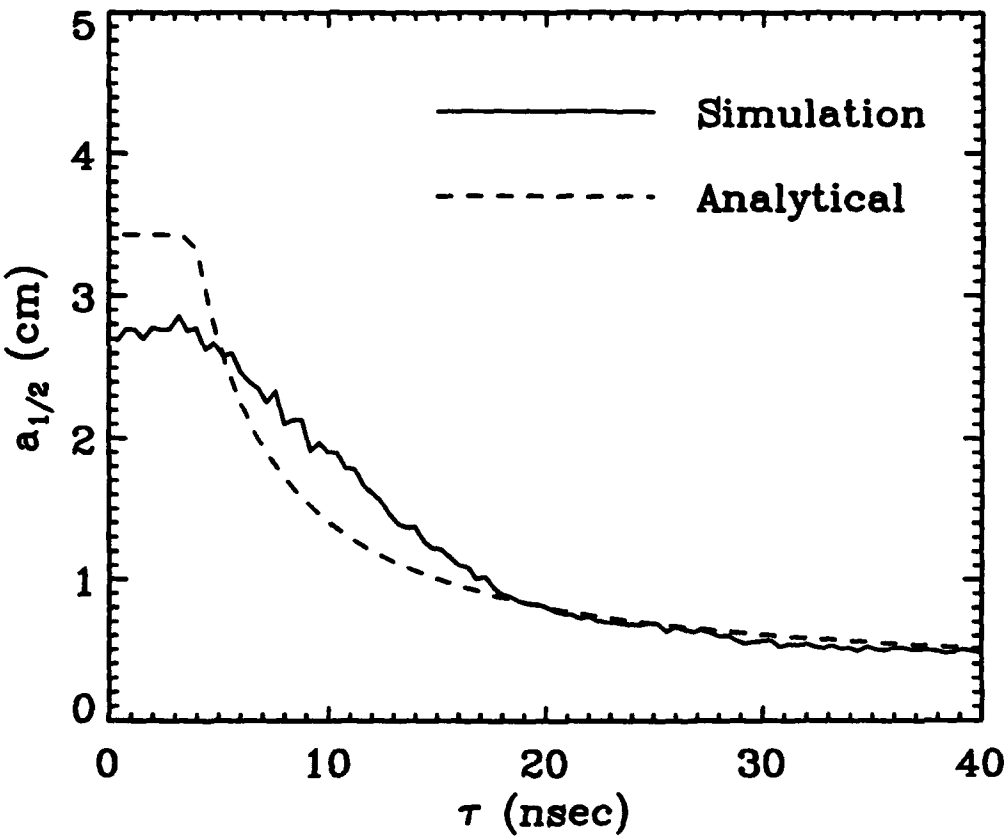

Figure 4

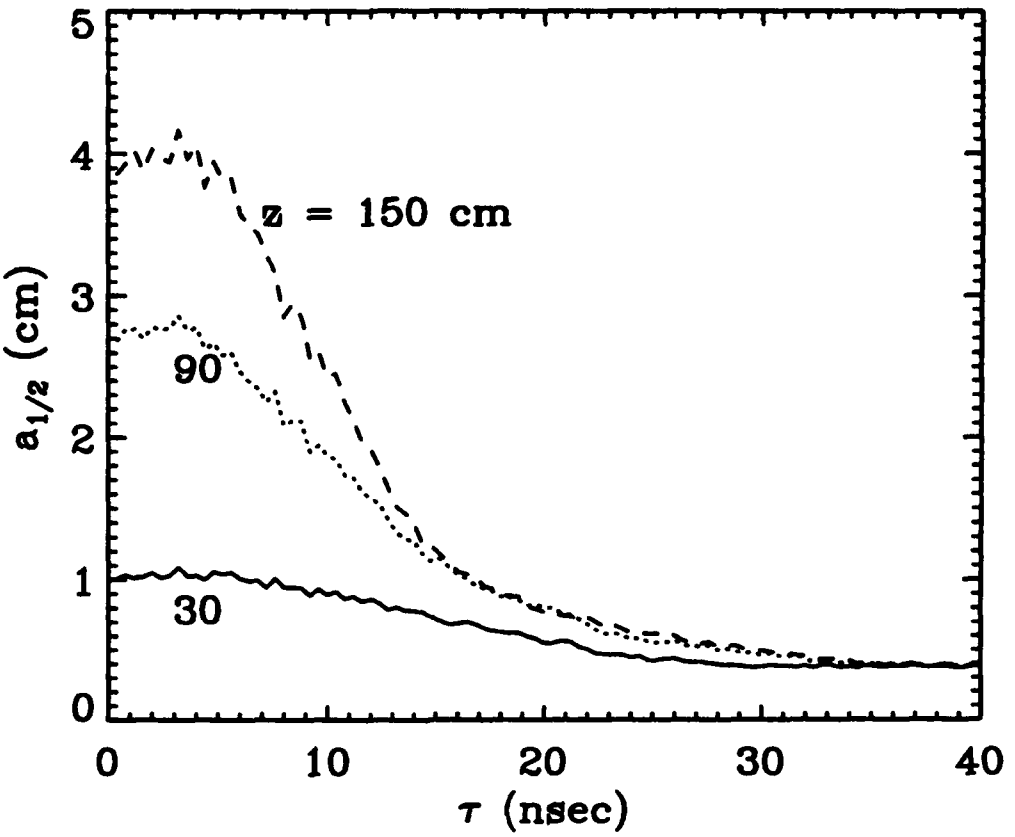

Figure 5

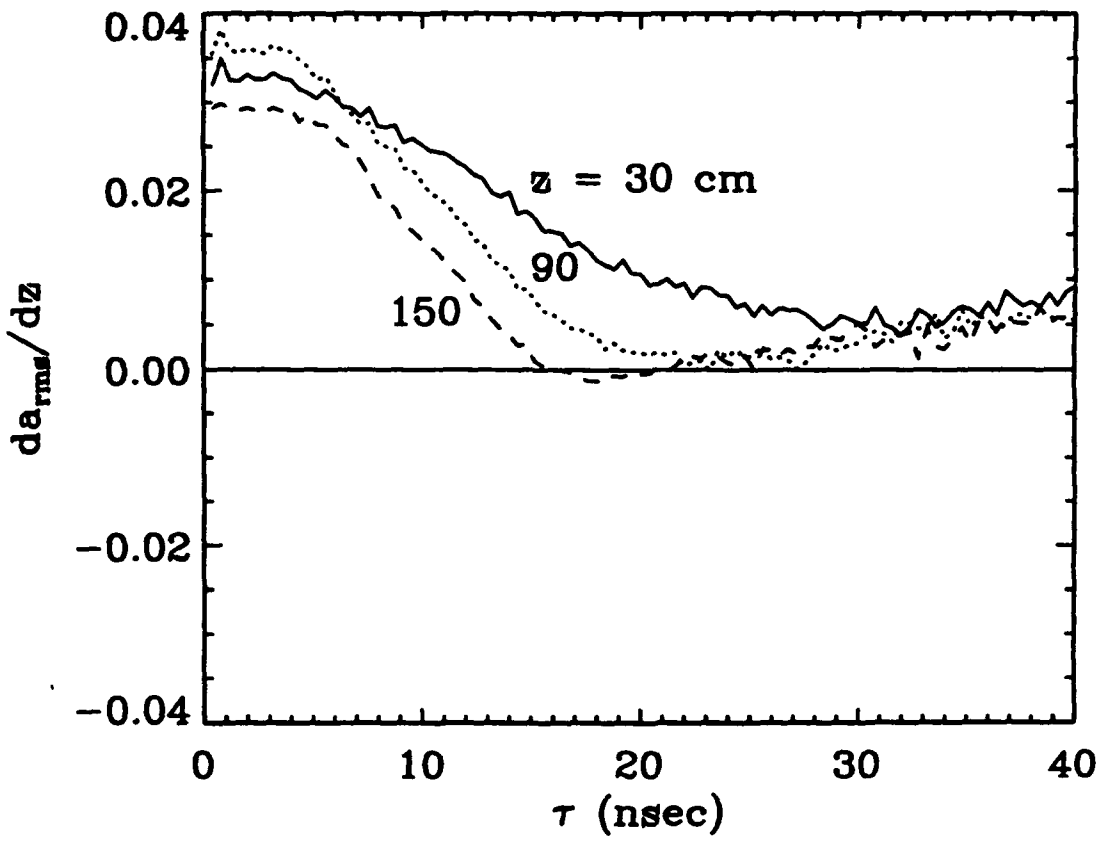

Figure 6

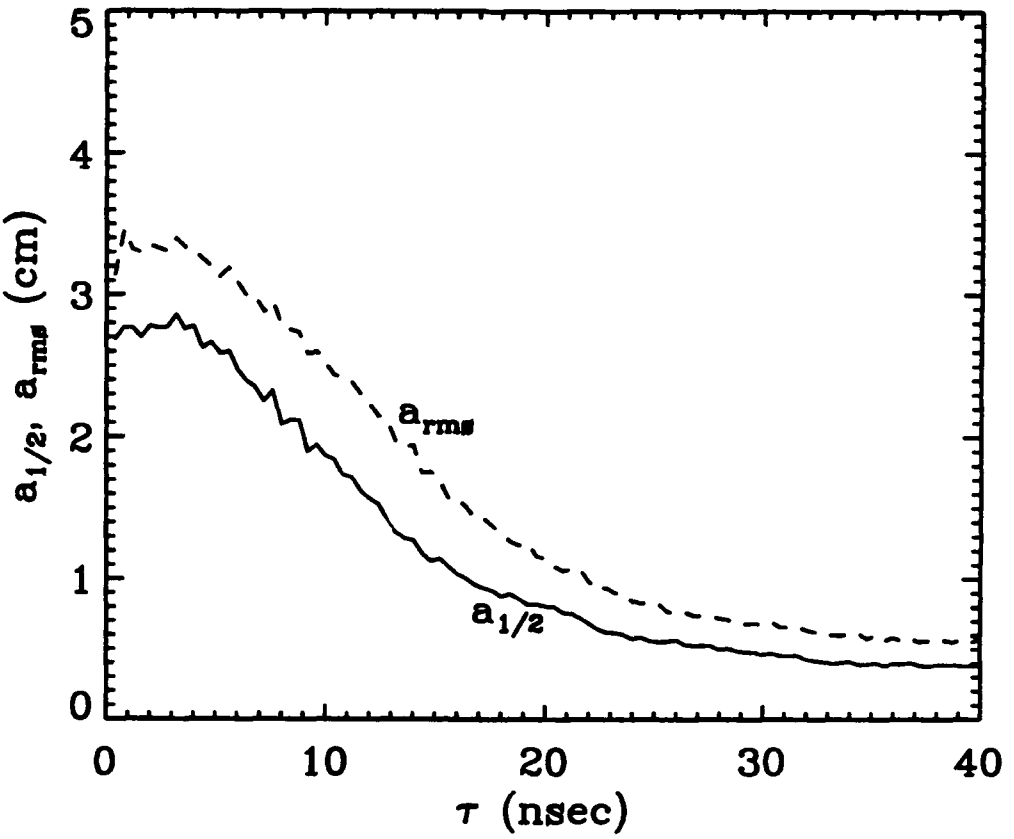

Figure 7

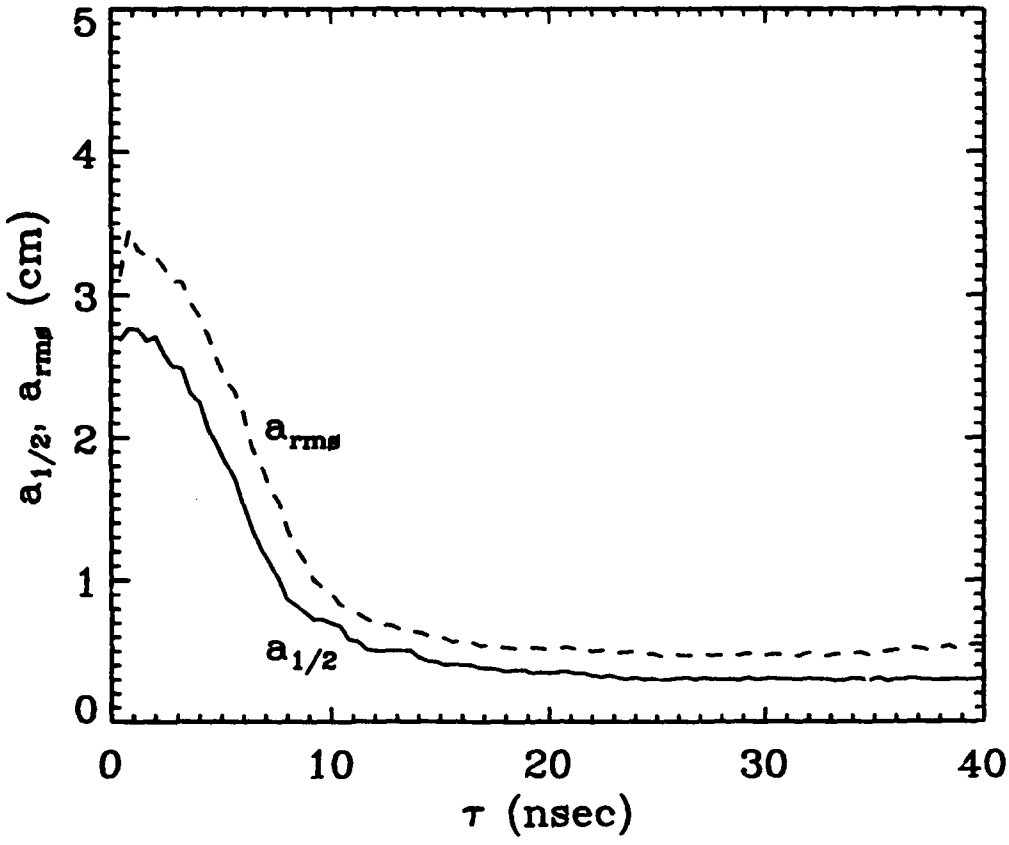

Figure 8

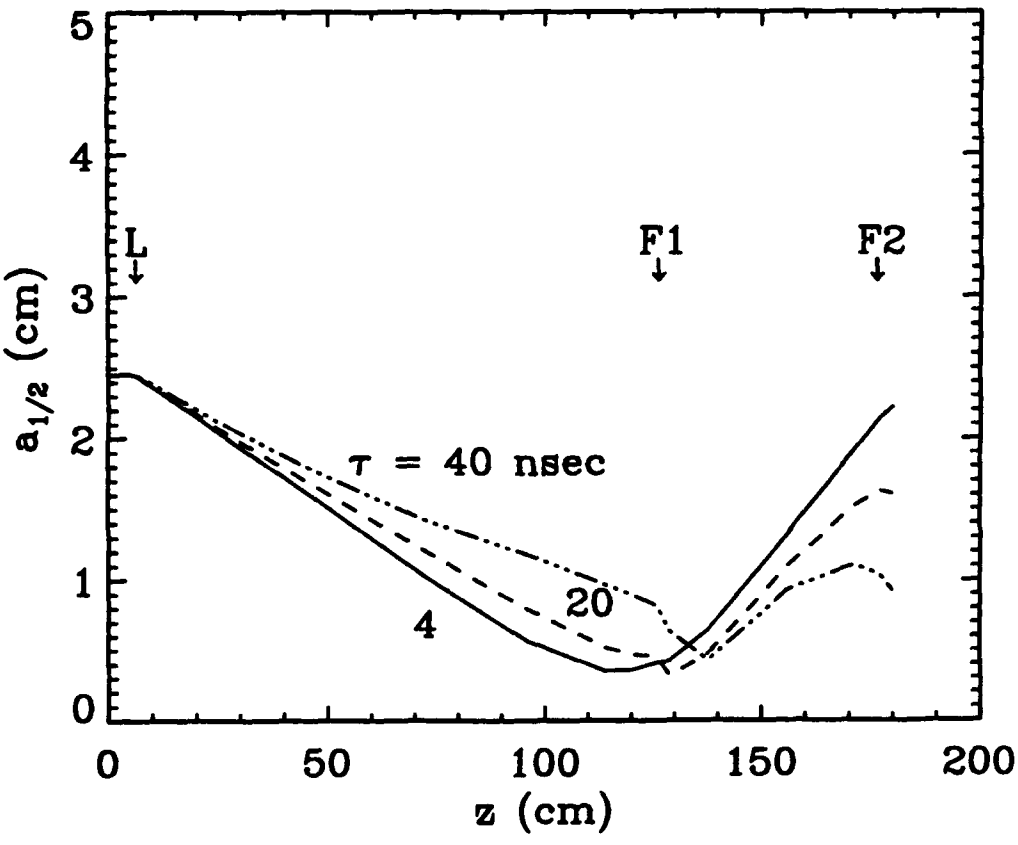

Figure 9

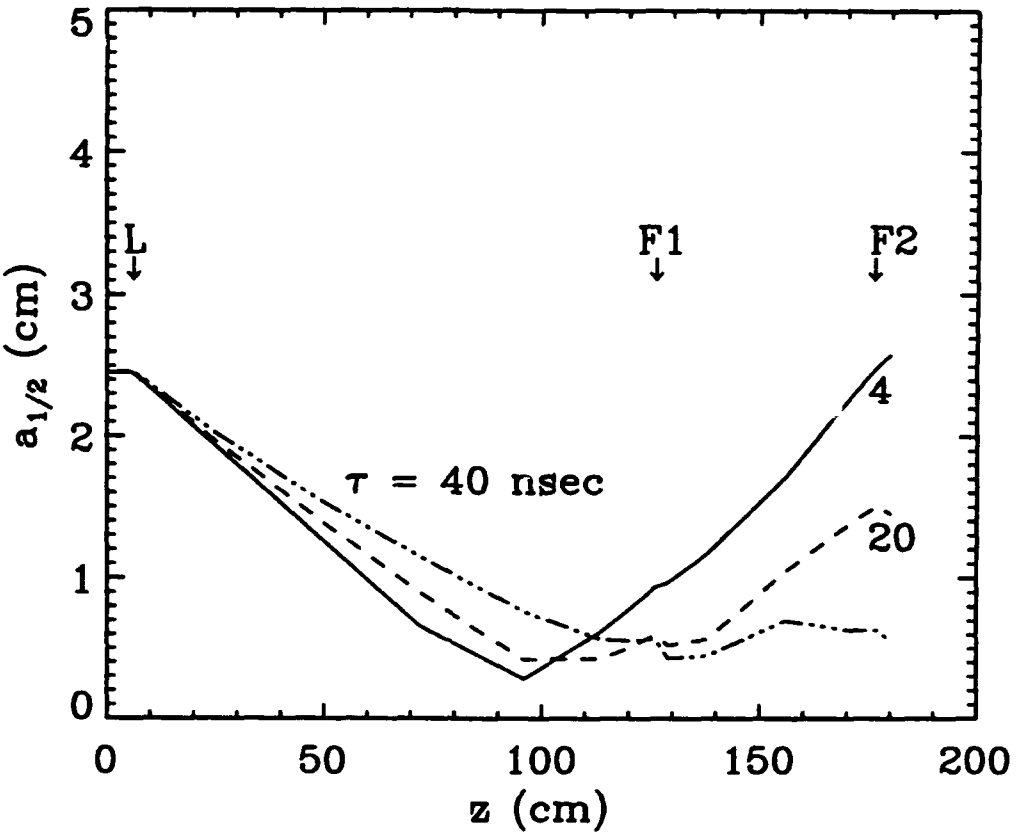

Figure 10

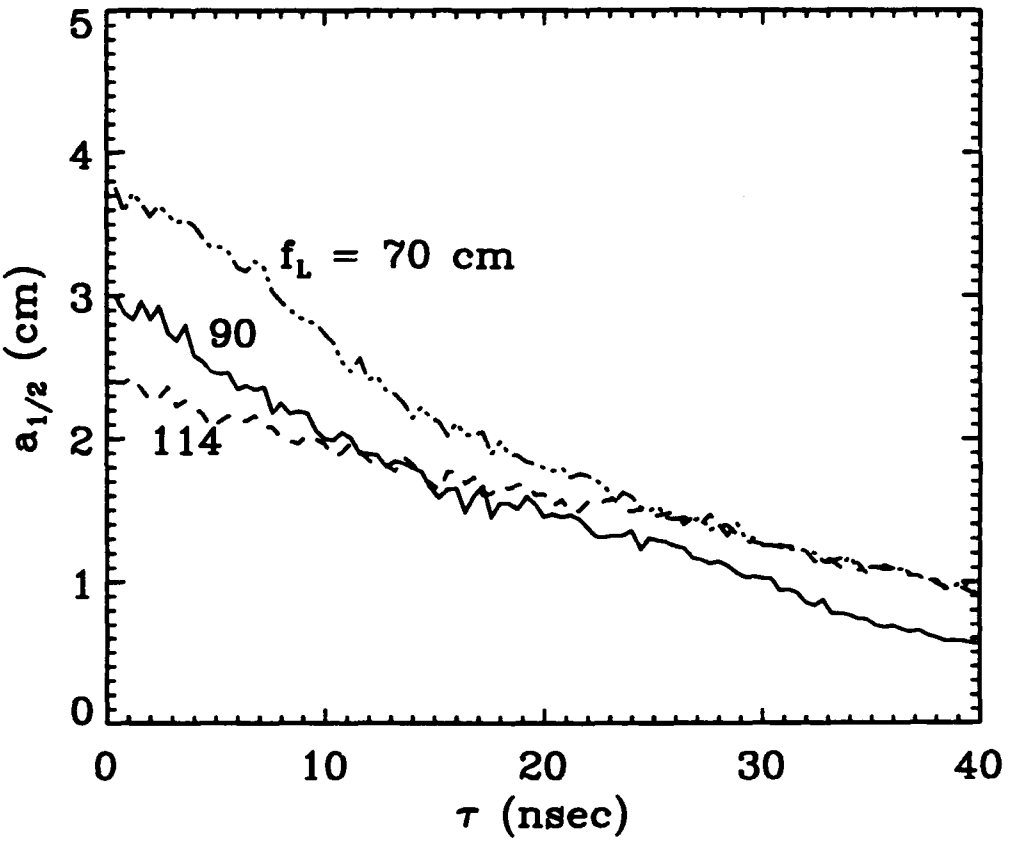

Figure 11

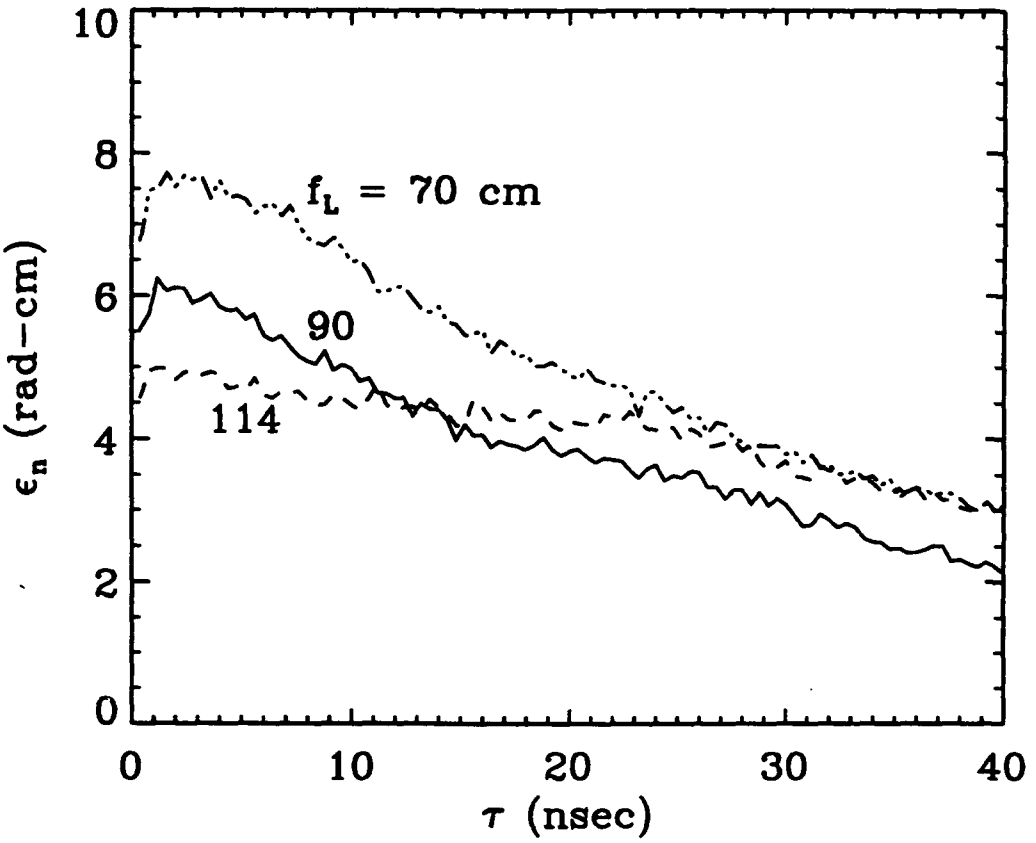

Figure 12

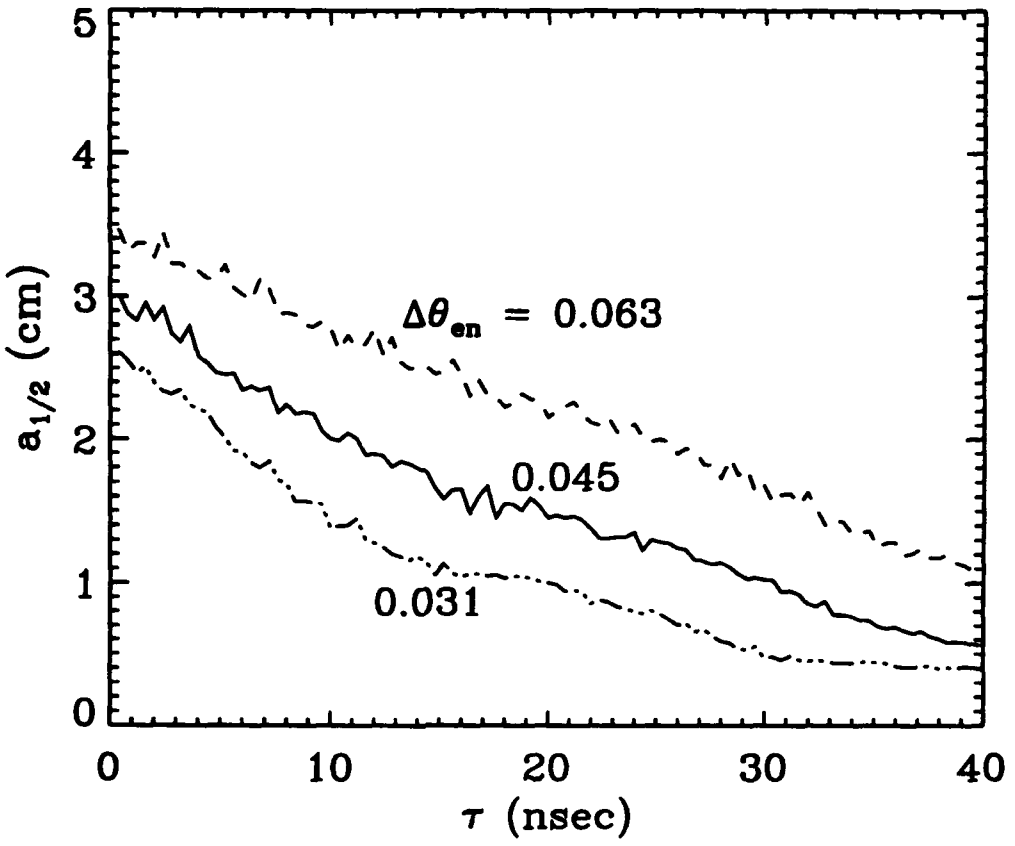
5
4
3
2
1
0
$a_{1/2}$ (cm)
$\Delta\theta_{en}$ = 0.063
0.045
0.031
0
10
20
30
40
τ (nsec)

Figure 13

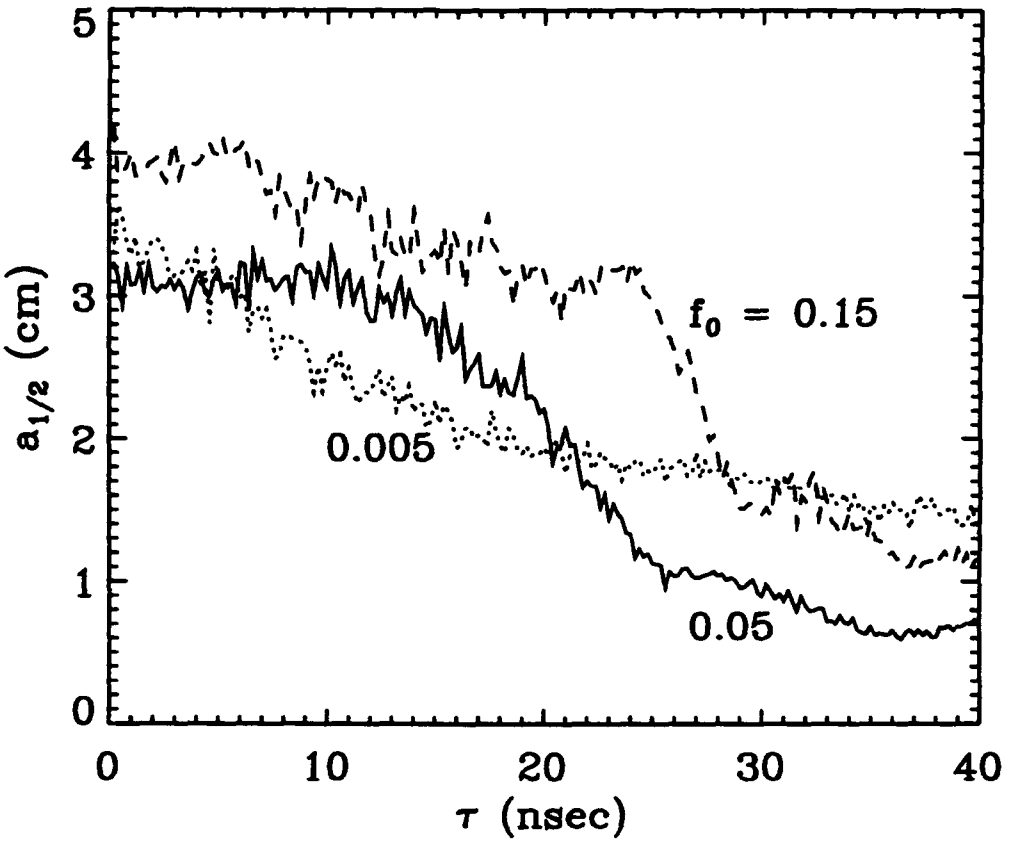

Figure 14

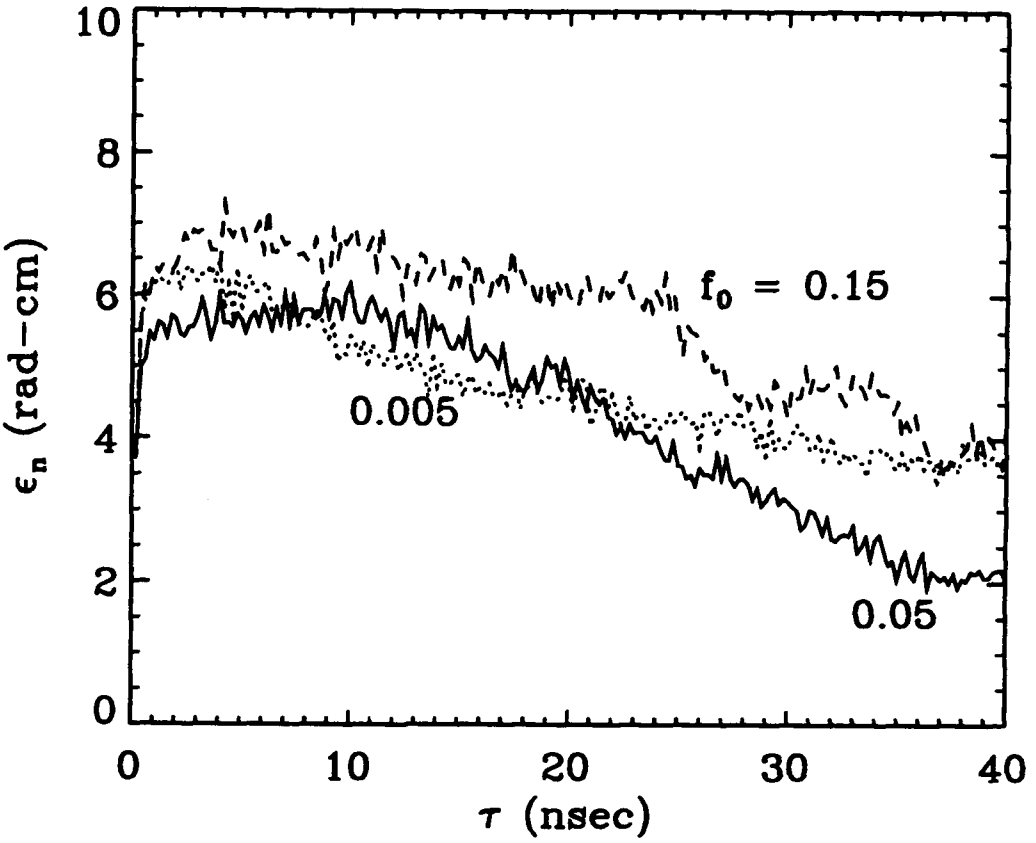

Figure 15

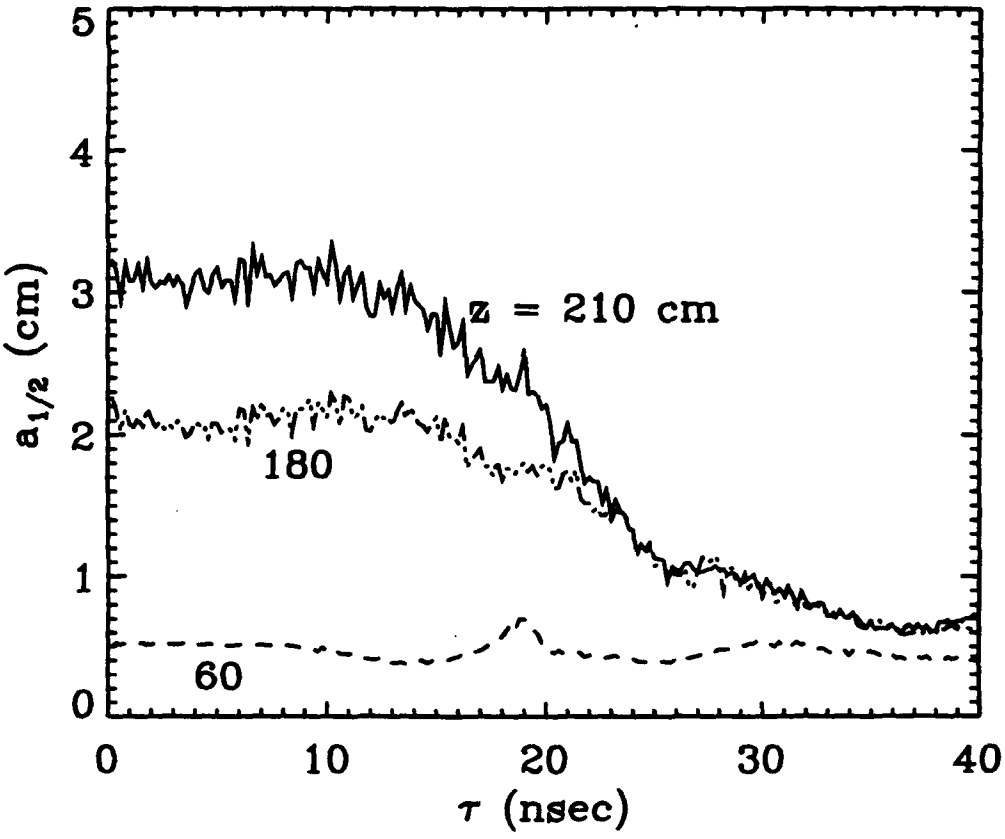

Figure 16

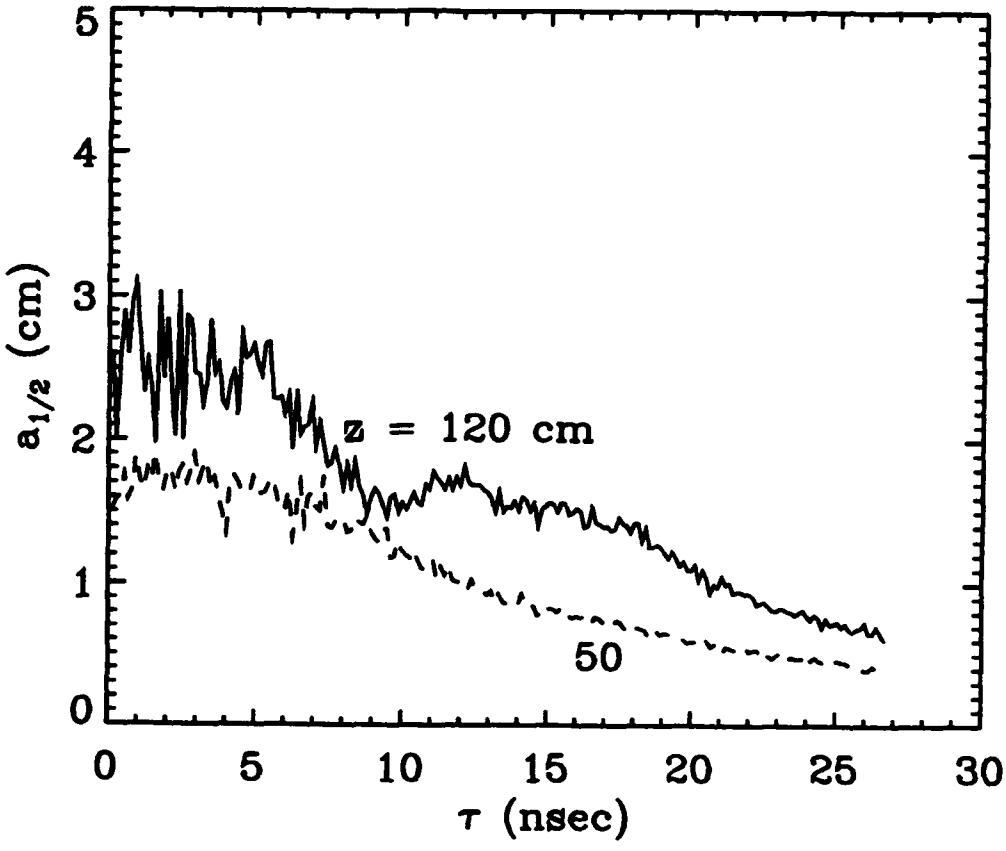

Figure 17

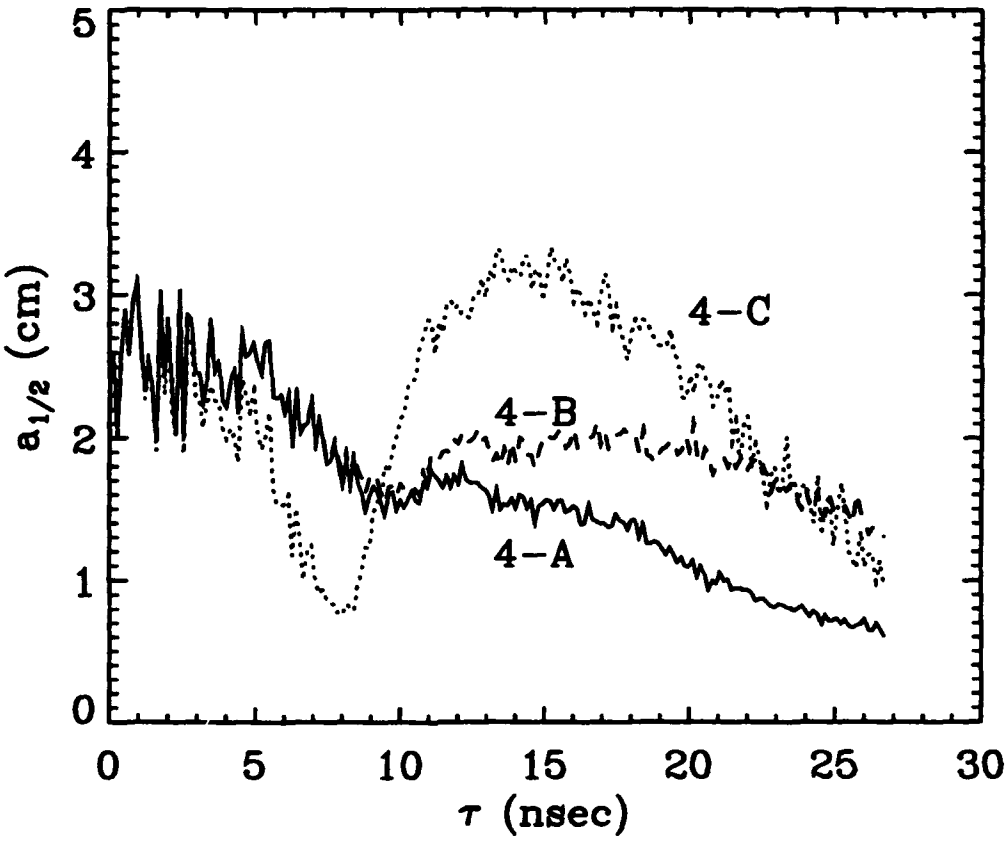

Figure 18

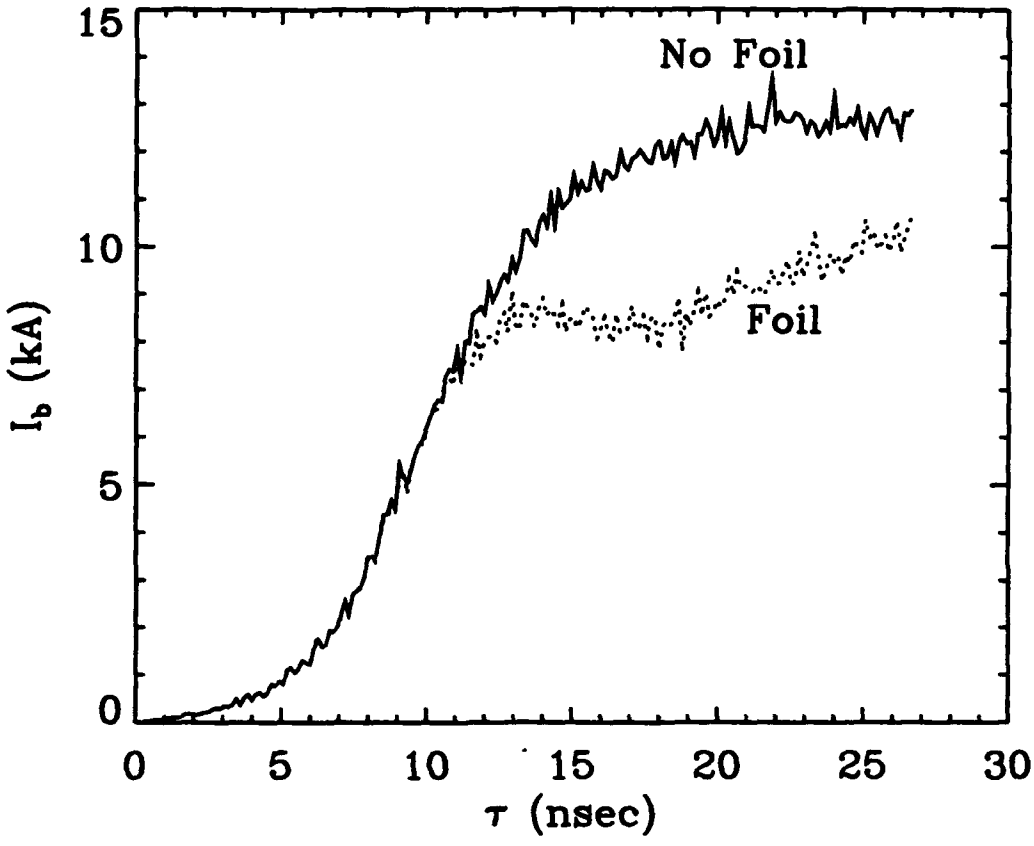

Figure 19